Published by Institute of Physics Publishing for SISSA

Received: *April 18, 2005*
Accepted: *July 1, 2005*
Published: *July 26, 2005*

Direct, indirect and collider detection of neutralino dark matter in SUSY models with non-universal Higgs masses

Howard Baer, Azar Mustafayev and Stefano Profumo

Department of Physics, Florida State University
Tallahassee, FL 32306, U.S.A.
E-mail: baer@hep.fsu.edu, mazar@hep.fsu.edu,profumo@hep.fsu.edu

Alexander Belyaev

Department of Physics and Astronomy, Michigan State University
East Lansing, MI 48824, U.S.A.
E-mail: belyaev@pa.msu.edu

Xerxes Tata

Department of Physics and Astronomy, University of Hawaii
Honolulu, HI 96822, U.S.A.
E-mail: tata@phys.hawaii.edu

Abstract: In supersymmetric models with gravity-mediated SUSY breaking, universality of soft SUSY breaking sfermion masses m_0 is motivated by the need to suppress unwanted flavor changing processes. The same motivation, however, does not apply to soft breaking Higgs masses, which may in general have independent masses from matter scalars at the GUT scale. We explore phenomenological implications of both the one-parameter and two-parameter non-universal Higgs mass models (NUHM1 and NUHM2), and examine the parameter ranges compatible with $\Omega_{CDM}h^2$, $BF(b \to s\gamma)$ and $(g-2)_\mu$ constraints. We have demonstrated that in contrast to the mSUGRA model, in both NUHM1 and NUHM2 models, the dark matter A-annihilation funnel can be reached at low values of $\tan\beta$, while the higgsino dark matter annihilation regions can be reached for low values of m_0. We show that there may be observable rates for indirect and direct detection of neutralino cold dark matter in phenomenologically aceptable ranges of parameter space. We also examine implications of the NUHM models for the Fermilab Tevatron, the CERN LHC and a $\sqrt{s} = 0.5 - 1\,\text{TeV}$ e^+e^- linear collider. Novel possibilities include: very light $\tilde{u}_R$, $\tilde{c}_R$ squark and $\tilde{e}_L$ slepton masses as well as light charginos and neutralinos and H, A and $H^\pm$ Higgs bosons.

Keywords: Hadron-Hadron Scattering, Dark Matter and Double Beta Decay, Neutrino Detectors and Telescopes, Supersymmetry Phenomenology.

Contents

1. Introduction

The minimal supergravity (mSUGRA) model [1] provides a convenient and popular template for exploration of many of the phenomenological consequences of weak scale supersymmetry [2]. In mSUGRA, it is assumed that supersymmetry is broken in a hidden sector of the model, with SUSY breaking communicated to the visible sector via gravitational interactions. The qualifier "minimal" in mSUGRA refers to the assumption of a flat Kähler metric, which leads to universal tree level scalar masses at some high energy scale, usually taken to be $Q = M_{GUT}$. The universality assumption ensures the super-GIM mechanism [3], which suppresses unwanted flavor-changing neutral current effects. An attractive feature of this framework is that electroweak symmetry can be radiatively broken (REWSB). This allows one to eliminate the superpotential $|\mu|$ parameter in favor of M_Z, and the low energy phenomenology is then determined by the well-known parameter space

$$\text{mSUGRA}: \quad m_0,\ m_{1/2},\ A_0,\ \tan\beta,\ \text{and sign}(\mu). \tag{1.1}$$

Here m_0 is the common GUT scale scalar mass, $m_{1/2}$ is the common GUT scale gaugino mass, A_0 is the common GUT scale trilinear term, $\tan\beta$ is the weak scale ratio of Higgs field vacuum expectation values, and μ is the superpotential Higgs mass term. We take $m_t = 178\,\mathrm{GeV}$ throughout this paper.

The mSUGRA model has been criticized because the assumption of universal scalar masses is *ad hoc* and does not follow from any known symmetry principle [4]. While it is possible to invoke an additional global U(N) symmetry for the (gravitational) interactions of the N chiral supermultiplets, this symmetry is clearly not respected by superpotential Yukawa couplings, and radiative corrections involving these Yukawa interactions can lead to large deviations from the universality hypothesis [5].

The assumption of equality of scalar masses receives partial support in Grand Unified Theories (GUTs). For instance, in SO(10) SUSY GUT models, all matter superfields of a single generation belong to a 16 dimensional spinor representation $\hat{\psi}(16)$ of SO(10), and their mass degeneracy is guaranteed if SUSY breaking masses are acquired above the SO(10) breaking scale. If the mechanism by which matter scalars acquire SUSY breaking masses is generation blind, universality of matter scalar masses would then obtain. In the case of minimal SO(10) SUSY GUTs, the two MSSM Higgs doublet superfields $\hat{H}_u$ and $\hat{H}_d$ belong to the same 10 dimensional fundamental representation $\hat{\phi}(10)$, so the corresponding SUSY breaking scalar mass terms would not be expected to be the same as those of the matter scalars. The phenomenologically desirable super-GIM mechanism would be ensured by requiring a U(3) symmetry amongst the different generations. In practice, the amount of degeneracy needed is greatest for the first two generations where FCNC constraints are the strongest, while the corresponding constraints for the third generation are rather mild [6]. The need for generational degeneracy can be further reduced if one invokes as well a degree of alignment between squark and quark mass matrices, or a (partial) decoupling solution to the SUSY flavor problem.

In this paper, we will maintain degeneracy amongst matter scalars at scales $Q \simeq M_{GUT}$, but will allow non-universality to enter the model via soft SUSY breaking masses for the Higgs scalars. In our analysis, we will differentiate between two cases for the non-universal Higgs mass (NUHM) models. Inspired by GUT models where both MSSM Higgs doublets are contained in a single superfield, we will first examine the NUHM model where $m_{H_u}^2 = m_{H_d}^2 \neq m_0^2$ at $Q = M_{GUT}$. In this case, we define the new parameter $m_\phi = \mathrm{sign}(m_{H_{u,d}}^2) \cdot \sqrt{|m_{H_{u,d}}^2|}$ at the GUT scale. Thus, the parameter space of this one parameter extension of the mSUGRA model is given by,

$$\text{NUHM1}: \qquad m_0,\ m_\phi,\ m_{1/2},\ A_0,\ \tan\beta \text{ and } \mathrm{sign}(\mu)\,. \tag{1.2}$$

The second case is inspired by GUT models where $\hat{H}_u$ and $\hat{H}_d$ belong to different multiplets. The parameter space for this second case is then given by

$$\text{NUHM2}: \qquad m_0,\ m_{H_u}^2,\ m_{H_d}^2,\ m_{1/2},\ A_0,\ \tan\beta \text{ and } \mathrm{sign}(\mu)\,. \tag{1.3}$$

The conditions of electroweak gauge symmetry breaking allows one to trade the GUT scale masses $m_{H_u}^2$ and $m_{H_d}^2$ for the weak scale parameters μ and m_A.

We remark that regardless of any theoretical motivation, if any small departure from a well-motivated framework such as mSUGRA causes significant differences in the phenomenological outcome, the new framework is worthy of examination. We will see below that enlarging the model parameter space to split off the GUT scale Higgs boson mass parameters from those of other scalars leads to significant departures from mSUGRA expectations upon the incorporation of the WMAP constraint on the relic density of cold dark matter. Motivated by this, our goal here is to explore in detail the phenomenological consequences of the NUHM1 and NUHM2 models. Before doing so, we note that the mSUGRA model has recently been tightly constrained by several measurements [7]. These include 1.) the combined measurement [8] of the branching fraction $BF(b \to s\gamma) = (3.25 \pm 0.37) \times 10^{-4}$, 2.) the measurement [9] of the deviation of the muon anomalous magnetic moment $\Delta a_\mu \equiv \Delta(g-2)_\mu/2 = (27 \pm 10) \times 10^{-10}$ from the SM prediction [10], and 3.) the WMAP determination of the relic density of cold dark matter (CDM) in the universe [11]: $\Omega_{CDM}h^2 = 0.113 \pm 0.009$. In addition, we invoke the usual constraint from LEP2 that charginos should have mass $m_{\widetilde{W}_1} \geq 103.5\,\mathrm{GeV}$. We remark that there could be significant theoretical uncertainties in the evaluation of both Δa_μ and, especially for large values of $\tan\beta$, also $BF(b \to s\gamma)$ so that any inferences from them should be interpreted with care. The first two constraints favor mSUGRA models with $\mu > 0$. The WMAP constraint restricts the mSUGRA parameter space to lie in one of the following regions [12–15]:

- the bulk region at low m_0 and low $m_{1/2}$, where neutralino annihilation in the early universe occurs predominantly via t-channel slepton exchange (this region is now essentially excluded by the combination of WMAP $\Omega_{CDM}h^2$ bound and the LEP2 bounds on $m_{\widetilde{W}_1}$ and m_h, save where it overlaps with the stau co-annihilation region),
- the stau co-annihilation at low m_0 but almost any $m_{1/2}$ value, where $m_{\widetilde{Z}_1} \simeq m_{\tilde{\tau}_1}$ [16], or the stop co-annihilation region for special values of A_0 where $m_{\widetilde{Z}_1} \simeq m_{\tilde{t}_1}$ [17],
- the hyperbolic branch/focus point region (HB/FP) at large m_0, where $|\mu|$ becomes small, and the neutralino develops a significant higgsino component [18–20], and
- the A-annihilation funnel at large $\tan\beta$, where $2m_{\widetilde{Z}_1} \sim m_A$, and neutralino annihilation in the early universe occurs via the broad A and H Higgs boson resonances [21]. A light Higgs resonance annihilation region may also be possible at low $m_{1/2}$ values where $2m_{\widetilde{Z}_1} \simeq m_h$ [22].

Throughout this work, we use Isajet 7.72 to generate sparticle mass spectra [23], IsaReD [13] for the relic density calculation, and the `DarkSUSY` package [24] for the computation of dark matter detection rates.

At this point, we would like to take note of a variety of earlier studies of models with non-universal Higgs masses. SUGRA models with non-universal Higgs masses were first studied by Berezinski et al., who focussed on direct detection of neutralino dark matter [27] and indirect detection via neutrino telescopes [28]. Around the same time, direct detection of neutralino dark matter in NUHM models was also investigated by Arnowitt and

Nath [29], and subsequently by Bottino et al.[30]. These latter papers explored only the case of positive squared Higgs masses. Bottino et al. explored direct DM detection for cases including negative squared Higgs masses in ref. [31]. Ellis et al. [32] made a thorough exploration of parameter space of the NUHM2 model using the μ and m_A variables, and investigated direct detection rates in ref. [33]. Indirect detection via neutrinos was investigated by Barger *et al.*[34] for models with universality and non-universality. Recently, both direct [35] and indirect [36] detection of neutralino dark matter has been investigated by Munoz et al. in the context of models with *both* scalar and gaugino mass non-universality.

Our present study goes beyond these previous works in several respects:

1. we investigate the more constrained NUHM1 model in section 2, and show for the first time that in this minimal (one parametric extension) of mSUGRA model there are always *two solutions for low relic density*: one is neutralino annihilation via heavy Higgs resonance even at low values of $\tan\beta$ while the other is neutralino annihilation via higgsino components at low values of m_0;

2. we find new allowed regions of the NUHM2 model — the light squark/slepton co-annihilation regions as discussed in section 3;

3. we investigate direct and indirect detection of neutralino dark matter, including anti-matter, neutrino and gamma ray indirect searches for the new parameter regions mentioned above;

4. for the first time, we consider the implications of the NUHM1 and NUHM2 models for collider searches at the Fermilab Tevatron, CERN LHC and ILC linear e^+e^- colliders, and show how these correlate with the direct and indirect dark matter searches. In this connection, we also emphasize the sensitivity of the implications of the WMAP measurement of $\Omega_{CDM}h^2$ for collider expectations to the underlying framework. In particular, we show that inferences valid in the mSUGRA model may simply be invalid in the extended NUHM framework.

The remainder of this paper is organized as follows. In section 2, we explore the allowed regions of the NUHM1 model which was first studied in ref. [25]. We will find that even for low values of m_0, *raising* the ratio m_ϕ/m_0 brings us into the low $|\mu|$ region where the relic density is in accord with the WMAP allowed range; this is quite unlike the situation in mSUGRA where the higgsino annihilation region occurs only at multi-TeV values of m_0. In addition, *lowering* the ratio m_ϕ/m_0 into the range of *negative* values decreases the value of m_A until the A-annihilation funnel is reached. In this case, the A-funnel region can occur at *any* $\tan\beta$ value where an acceptable spectrum can be generated.

We introduce and outline in section 2.3 the computation of direct and indirect dark matter rates. We make use of consistent halo models in the attempt to systematically compare the reach in all various detection channels. We find enhanced signal rates for direct and indirect detection of neutralino cold dark matter in these WMAP-allowed regions [26].

JHEP07(2005)065

In section 2.5, we explore some unique consequences of the NUHM1 model for collider searches. In the higgsino region of the NUHM1 model, charginos and neutralinos all become rather light, and more easily accessible to collider searches. In addition, lengthy gluino and squark cascade decays to the various charginos and neutralinos occur, leading to the possibility of spectacular events at the CERN LHC. In the A-funnel region, the A, H and $H^{\pm}$ Higgs bosons may be kinematically accessible to searches at the International Linear Collider (ILC) or at the CERN LHC, and may also be present in gluino and squark cascade decays.

In section 3, we explore the NUHM2 model. In this case, since μ and m_A can now be used as input parameters, it is always possible to choose values such that one lies either in the higgsino annihilation region or in the A-funnel region, for any value of $\tan\beta$, m_0 or $m_{1/2}$ that gives rise to a calculable SUSY mass spectrum. In the low μ region, charginos and neutralinos are again likely to be light, and possibly accessible to Fermilab Tevatron, CERN LHC and ILC searches. If instead one is in the A-annihilation funnel, then the heavier Higgs scalars may be light enough to be produced at observable rates at hadron or lepton colliders. In addition, new regions are found where consistency with WMAP data is obtained because either $\tilde{u}_R$, $\tilde{c}_R$ squarks or left- sleptons become very light. The $\tilde{u}_R$ and $\tilde{c}_R$ co-annihilation region leads to large rates for direct and indirect detection of neutralino dark matter, and is in fact already constrained by searches from CDMS2. We present a summary and our conclusions in section 4.

2. NUHM1 model

2.1 Overview

In this section, we investigate the phenomenology of the NUHM1 model, wherein the Higgs masses $m_{H_u}^2 = m_{H_d}^2 \equiv \mathrm{sign}(m_\phi) \cdot |m_\phi|^2$ at $Q = M_{GUT}$, with $m_\phi^2 \neq m_0^2$. We first note that the parameter range for m_ϕ need not be limited to positive values at the GUT scale, and that, indeed, to achieve radiative EWSB, $m_{H_u}^2$ must evolve to negative values. Indeed, negative squared Higgs mass parameters (at $Q = M_{GUT}$) are predicted in the SU(5) fixed point scenario of ref. [37].

We also note that some authors impose so-called GUT stability (GS) bounds,

$$m_{H_u}^2(M_{GUT}) + \mu^2(M_{GUT}) > 0 \tag{2.1}$$

and

$$m_{H_d}^2(M_{GUT}) + \mu^2(M_{GUT}) > 0\,, \tag{2.2}$$

to avoid EWSB at too high a scale. The reliability of these bounds is debated in refs. [38]; here we will merely remark on regions of parameter space where they occur, and leave it to the reader to decide whether or not to impose them.

We show one of the critical aspects of the NUHM1 model in figure 1, where we plot the values of μ, m_A, $m_{\widetilde{Z}_1}$ and $2m_{\widetilde{Z}_1}$ versus m_ϕ while fixing $m_0 = m_{1/2} = 300\,\mathrm{GeV}$, with $A_0 = 0$, $\tan\beta = 10$ and $\mu > 0$. The region to the left of the dot-dashed line indicates where the GS bound fails. The curves terminate because electroweak symmetry breaking

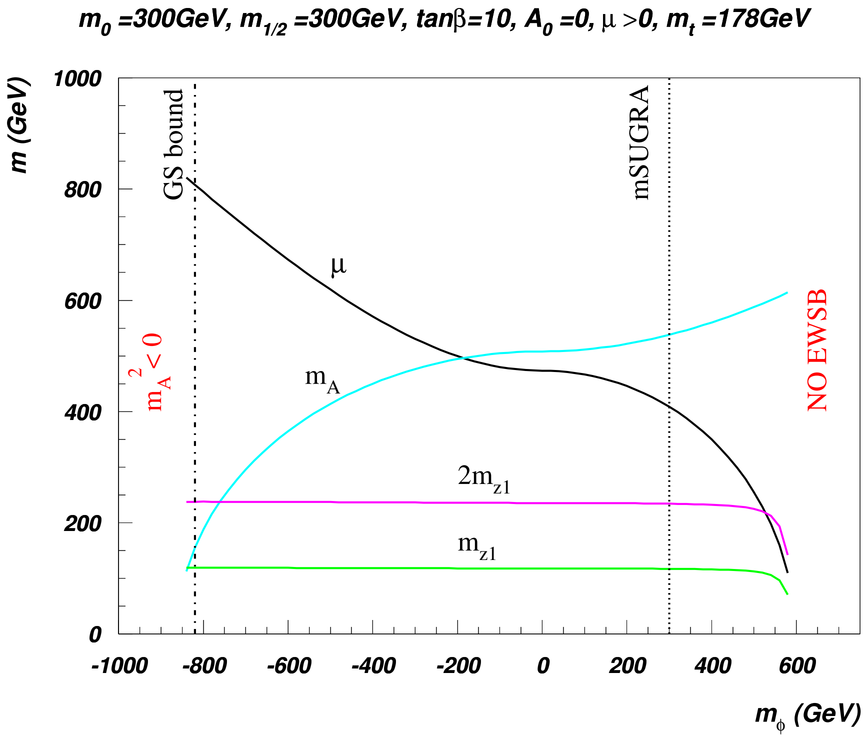

Figure 1: Plot of μ, m_A and $m_{\widetilde{Z}_1}$ vs. m_ϕ for $m_0 = 300\,\mathrm{GeV}$, $m_{1/2} = 300\,\mathrm{GeV}$, $A_0 = 0$, $\tan\beta = 10$ and $m_t = 178\,\mathrm{GeV}$. We take $\mu > 0$.

is not obtained as marked on the figure: in fact, on the right, where $|\mu|$ becomes small, the chargino mass falls below the LEP bound just before the EWSB constraint kicks in. The black curve denotes the value of the μ parameter, which takes a value of $\mu = 409\,\mathrm{GeV}$ for $m_\phi = 300\,\mathrm{GeV}$ (the mSUGRA case). The parameter μ becomes much larger for $m_\phi < -m_0$, and much smaller for $m_\phi > m_0$ [39]. The region of small μ is of particular interest since in that case the lightest neutralino develops substantial higgsino components, and leads to a relic density which can be in accord with the WMAP determination. In contrast, in the mSUGRA model the higgsino-LSP region occurs in the HB/FP region, which occurs at very large m_0 values of order several TeV (depending somewhat on the assumed value of m_t). The HB/FP region has been criticized in the literature in that the large m_0 values may lead to large fine-tunings [40] (for an alternative point of view, see refs. [18] and [19]). This illustrates an important virtue of the NUHM1 model: the higgsino annihilation region may be reached even with *arbitrarily low* values of m_0 and $m_{1/2}$, provided of course that sparticle search bounds are respected.

We also see from figure 1 that the value of m_A can range beyond its mSUGRA value for large values of m_ϕ, to quite small values when m_ϕ becomes less than zero. In particular, when $m_A \sim 2m_{\widetilde{Z}_1}$, neutralinos in the early universe may annihilate efficiently through the A and H Higgs resonances, so that again $\Omega_{CDM}h^2$ may be brought into accord with the WMAP result. In the mSUGRA model, the A-annihilation funnel occurs only at large $\tan\beta \sim 45-55$. However, in the NUHM1 model, the A-funnel region may be reached even for low $\tan\beta$ values if m_ϕ is taken to be sufficiently negative.

To understand the behavior of the μ parameter and m_A in the NUHM1 model, we first examine the renormalization group equations (RGEs) for the soft SUSY breaking Higgs squared mass parameters. Neglecting the Yukawa couplings for the first two generations, these read:

$$\frac{dm^2_{H_u}}{dt} = \frac{2}{16\pi^2}\left(-\frac{3}{5}g_1^2M_1^2 - 3g_2^2M_2^2 + \frac{3}{10}g_1^2S + 3f_t^2X_t\right), \tag{2.3}$$

$$\frac{dm^2_{H_d}}{dt} = \frac{2}{16\pi^2}\left(-\frac{3}{5}g_1^2M_1^2 - 3g_2^2M_2^2 - \frac{3}{10}g_1^2S + 3f_b^2X_b + f_\tau^2X_\tau\right), \tag{2.4}$$

where $t = \log(Q)$, $f_{t,b,\tau}$ are the t, b and τ Yukawa couplings, and

$$X_t = m^2_{Q_3} + m^2_{\tilde{t}_R} + m^2_{H_u} + A_t^2, \tag{2.5}$$

$$X_b = m^2_{Q_3} + m^2_{\tilde{b}_R} + m^2_{H_d} + A_b^2, \tag{2.6}$$

$$X_\tau = m^2_{L_3} + m^2_{\tilde{\tau}_R} + m^2_{H_d} + A_\tau^2, \quad \text{and} \tag{2.7}$$

$$S = m^2_{H_u} - m^2_{H_d} + Tr\left[\mathbf{m}_Q^2 - \mathbf{m}_L^2 - 2\mathbf{m}_U^2 + \mathbf{m}_D^2 + \mathbf{m}_E^2\right]. \tag{2.8}$$

The term S is identically zero in the NUHM1 model, but can be non-zero in the NUHM2 model.

For small-to-moderate values of $\tan\beta$, $f_t \gg f_b,\ f_\tau$, and so the RGE terms including X_t usually dominate the X_b and X_τ terms. The RGE terms including Yukawa couplings occur with overall positive signs, which results in driving the corresponding soft Higgs boson mass squared parameters to smaller (and ultimately negative) values at the low scale. Indeed, this is the familiar REWSB mechanism. Since $X_t \ni m^2_{H_u}$, a large, positive value of $m_\phi > m_0$ results in a stronger push of $m^2_{H_u}$ to negative values (relative to that in mSUGRA) during the running from M_{GUT} to M_{weak}, while the evolution of $m^2_{H_d}$ is rather mild. Alternatively, if $m_\phi \ll 0$, then there exist cancellations within the X_t term which results in a milder running of $m^2_{H_u}$ from M_{GUT} to M_{weak}. Indeed, as shown in ref. [25],

$$\Delta m^2_{H_{u,d}} \equiv m^2_{H_{u,d}}(\text{NUHM1}) - m^2_{H_{u,d}}(\text{mSUGRA})$$

satisfies

$$\Delta m^2_{H_u}(\text{weak}) \simeq \Delta m^2_{H_u}(\text{GUT}) \times e^{-J_t}, \tag{2.9}$$

where

$$J_t = \frac{3}{8\pi^2}\int dt f_t^2 > 0,$$

with f_t being the top quark Yukawa coupling. We see that Δm_{H_u} maintains its sign, but reduces in magnitude under evolution from the GUT to the weak scale. The same argument applies for $\Delta m^2_{H_d}$, except that the effect of evolution is much smaller because $f_{b,\tau} \ll f_t$ except when $\tan\beta$ is very large. The situation is illustrated in figure 2, where we plot the running of $m^2_{H_u}$ and $m^2_{H_d}$ from M_{GUT} to M_{weak} using the same model parameters as in figure 1, except for three choices of $m_\phi = 500$ GeV, 300 GeV (mSUGRA case) and -700 GeV. In these cases, the weak scale values of $m^2_{H_u}$ are $-(251\text{ GeV})^2$, $-(407\text{ GeV})^2$ and $-(732\text{ GeV})^2$, respectively, while the corresponding weak scale values of $m^2_{H_d}$ are $(527\text{ GeV})^2$, $(348\text{ GeV})^2$ and $-(672\text{ GeV})^2$.

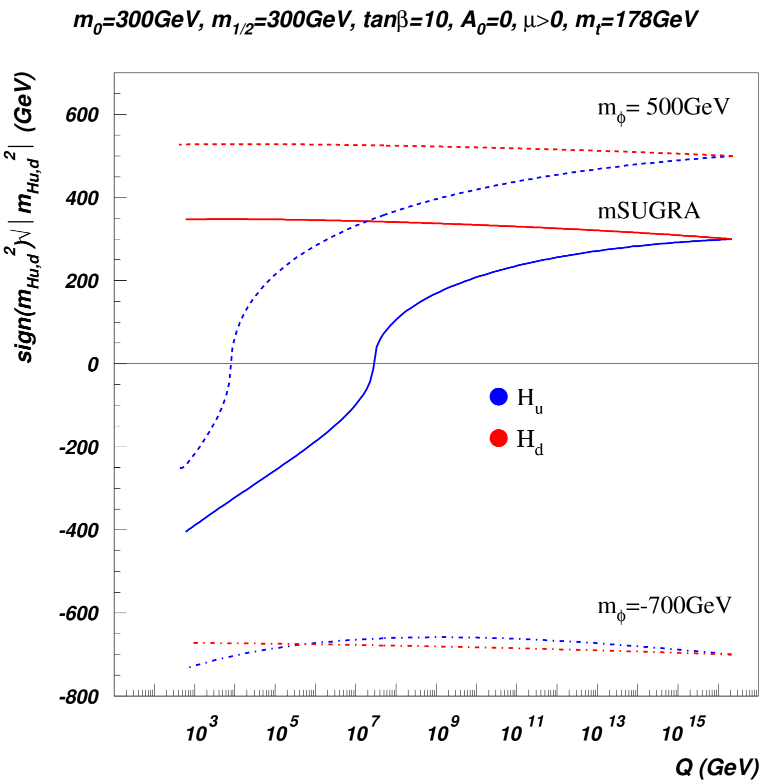

Figure 2: The evolution of $m_{H_u}^2$ and $m_{H_d}^2$ from $Q = M_{GUT}$ to M_{weak} for $M_\phi = 300$ GeV (mSUGRA case), 500 GeV and -700 GeV. We also take $m_0 = 300\,\text{GeV}$, $m_{1/2} = 300\,\text{GeV}$, $A_0 = 0$, $\tan\beta = 10$ and $m_t = 178\,\text{GeV}$, with $\mu > 0$.

The tree level minimization condition for EWSB in the MSSM is

$$\mu^2 = \frac{m_{H_d}^2 - m_{H_u}^2 \tan^2\beta}{(\tan^2\beta - 1)} - \frac{M_Z^2}{2}\,. \tag{2.10}$$

For moderate to large values of $\tan\beta$ (as favored by LEP2 Higgs boson mass constraints), and $|m_{H_u}| \gg M_Z$, $\mu^2 \sim -m_{H_u}^2$. Thus, we see that in the case of large negative m_ϕ values, we would expect a large $|\mu|$ parameter, whereas for large positive m_ϕ values, $m_{H_u}^2$ is barely driven to negative values, and we expect a small $|\mu|$ parameter. Within the same approximation, the tree level pseudoscalar Higgs mass m_A is given by

$$m_A^2 = m_{H_u}^2 + m_{H_d}^2 + 2\mu^2 \simeq m_{H_d}^2 - m_{H_u}^2\,. \tag{2.11}$$

For large negative values of m_ϕ, the weak scale values of $m_{H_u}^2$ and $m_{H_d}^2$ are both negative, and can cancel against the $2\mu^2$ term, yielding small pseudoscalar masses. Meanwhile, for large positive values of m_ϕ, $m_{H_d}^2 \sim \text{sign}(m_\phi)m_\phi^2$ while $m_{H_u}^2$ is small, but negative. In this case there is no cancellation in the computation of m_A^2, and thus we expect m_A to be large, as shown in figure 1.

In figure 3, we show how different sparticle masses vary with m_ϕ for the same parameter choices as in figure 1. Most sparticle masses are relatively invariant to changes in m_ϕ. One

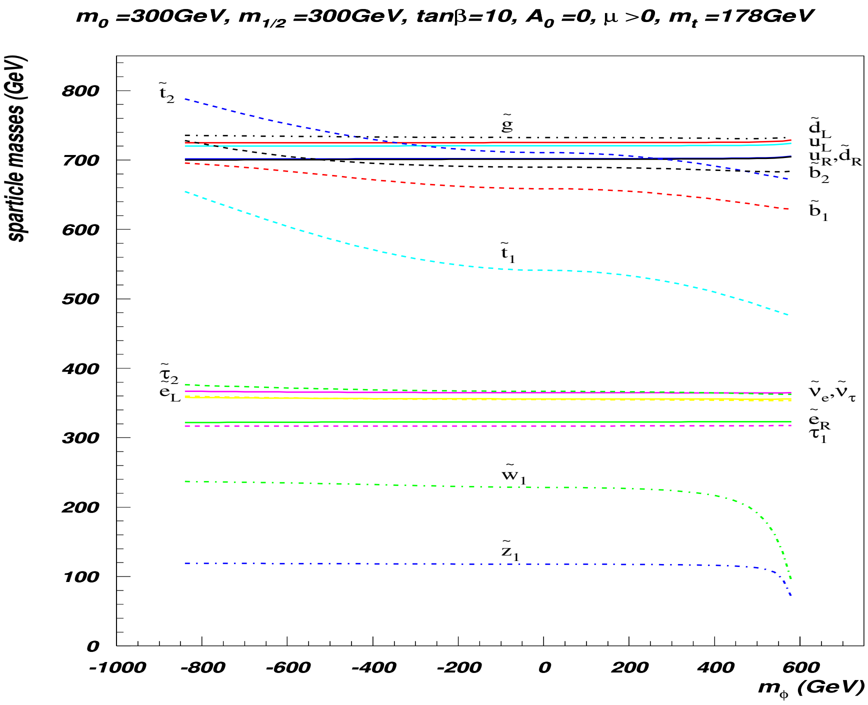

Figure 3: Various sparticle masses versus m_ϕ in the NUHM1 model for $m_0 = 300\,\mathrm{GeV}$, $m_{1/2} = 300\,\mathrm{GeV}$, $A_0 = 0$, $\tan\beta = 10$ and $m_t = 178\,\mathrm{GeV}$. We take $\mu > 0$.

exception occurs for the $\widetilde{W}_1$ and $\widetilde{Z}_{1,2}$ masses, which become small when $\mu \lesssim M_2$, and the $\widetilde{Z}_1$ becomes increasingly higgsino-like. The other exception occurs for the $\tilde{t}_{1,2}$ and $\tilde{b}_{1,2}$ masses. In this case, the $Q_3 \equiv (\tilde{t}_L, \tilde{b}_L)$ and $\tilde{t}_R$ running masses also depend on terms including $f_t^2 X_t$. Thus, when X_t is small (for $m_\phi < m_0$), the diagonal entries in the top and bottom squark mass squared matrices are not as suppressed due to top Yukawa coupling effects as in the mSUGRA case. In contrast, for large positive values of m_ϕ, X_t is large and these soft masses are more suppressed resulting lighter third generation squarks. These expectations are indeed born out in figure 3.

2.2 NUHM1 model: parameter space

The mSUGRA parameter space point we have used for illustration so far,

$$(m_0,\ m_{1/2},\ A_0,\ \tan\beta = 300\ \mathrm{GeV}, 300\ \mathrm{GeV}, 0, 10)$$

with $\mu > 0$ and $m_t = 178\,\mathrm{GeV}$, is excluded since $\Omega_{\widetilde{Z}_1} h^2 = 1.2$. However, by extending the parameter space to include m_ϕ as in the NUHM1 model, these parameter values are allowed for an appropriate choice of m_ϕ. As an example, in figure 4 we use $m_0, m_{1/2}$ and A_0 as in the mSUGRA parameter set above, and scan over $\tan\beta$ and m_ϕ values.

In plotting points, we construct a χ^2 value out of the three quantities $\Omega_{\widetilde{Z}_1} h^2$, $BF(b \to s\gamma)$ and Δa_μ, where $\chi^2 = \sum_{i=1}^{3} \frac{(x_i - \mu_i)^2}{\sigma_i^2}$, where x_i is the predicted value, μ_i is the measured value, and σ_i is the error on the ith measured quantity. In constructing the χ^2 value, we

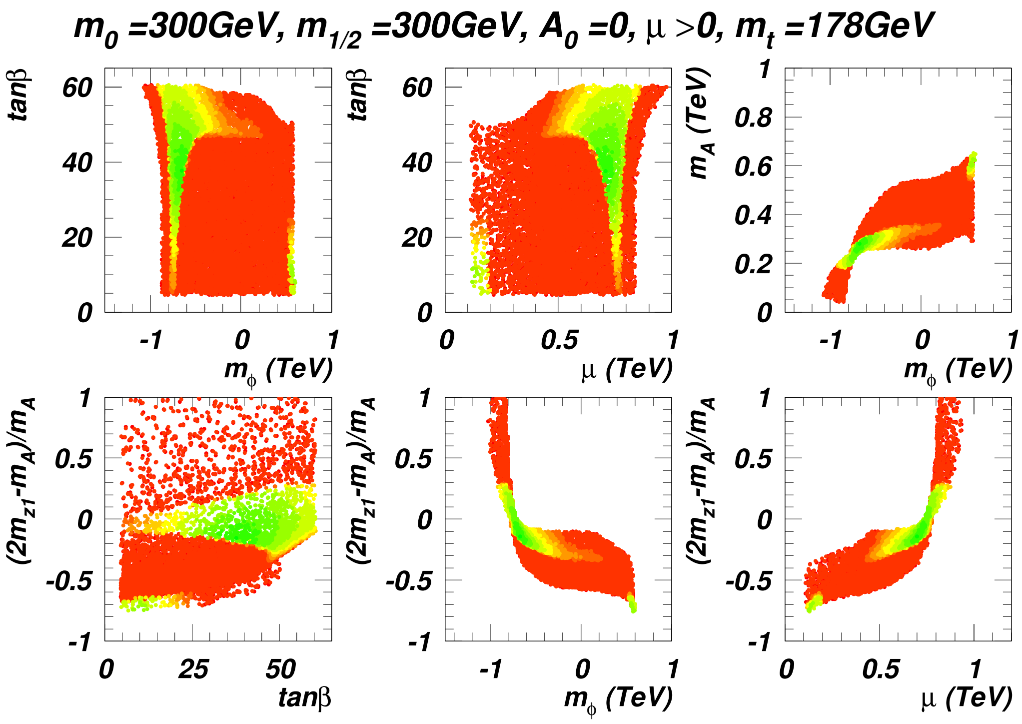

Figure 4: Ranges of $\sqrt{\chi^2}$ in a scan over $\tan\beta$ and m_ϕ values in the NUHM1 model for fixed $m_0 = m_{1/2} = 300$ GeV, $A_0 = 0$, $\mu > 0$ and $m_t = 178$ GeV. The green region corresponds to low values of $\sqrt{\chi^2} \lesssim \sqrt{3}$, while the red region has $\sqrt{\chi^2} \gtrsim 5$, with the yellow region corresponding to intermediate values.

only use the WMAP upper bound (thus, points with $\Omega_{\widetilde{Z}_1}h^2 < 0.113$ do not contribute to the χ^2) to allow for the possibility of mixed cold dark matter, where for instance a portion of dark matter might consist of, say, axions.[1] Green points have low $\sqrt{\chi^2} \lesssim \sqrt{3}$ values, and agree well with the central values of each of these measurements. Red points have large $\sqrt{\chi^2} \gtrsim 5$, and are excluded. Yellow points have intermediate values of $\sqrt{\chi^2}$. We show six frames illustrating various correlations amongst parameters. In frame *a*) showing m_ϕ vs. $\tan\beta$, we see the green/yellow A-annihilation funnel for $m_\phi \sim -0.8$ TeV, which occurs for *every* $\tan\beta$ value. We also see at $m_\phi \sim 0.6$ TeV the appearance of the higgsino region, corresponding to the HB/FP region of the mSUGRA model. While the relic density is in accord with WMAP in this region, as $\tan\beta$ increases, $BF(b \to s\gamma)$ and Δa_μ also increase, so that the higgsino region becomes increasingly disfavored for large $\tan\beta$. Frame *b*) shows the $\tan\beta$ vs. μ correlation, where we see that indeed μ is small in the higgsino region, and large in the A-funnel. Frame *c*) shows the m_ϕ vs. m_A correlation, and indeed we see large values of m_A in the higgsino region, while $m_A \sim 250$ GeV in the A-funnel. The remaining three frames show $(2m_{\widetilde{Z}_1} - m_A)/m_A$ vs. $\tan\beta$, m_ϕ and μ respectively, which explicitly displays the A-annihilation funnel against the input parameters and μ.

[1] A low thermal relic abundance may also be compatible with a fully supersymmetric dark matter scenario provided non-thermal production of neutralinos or cosmological enhancements of the thermal relic density occur: see section 2.3.

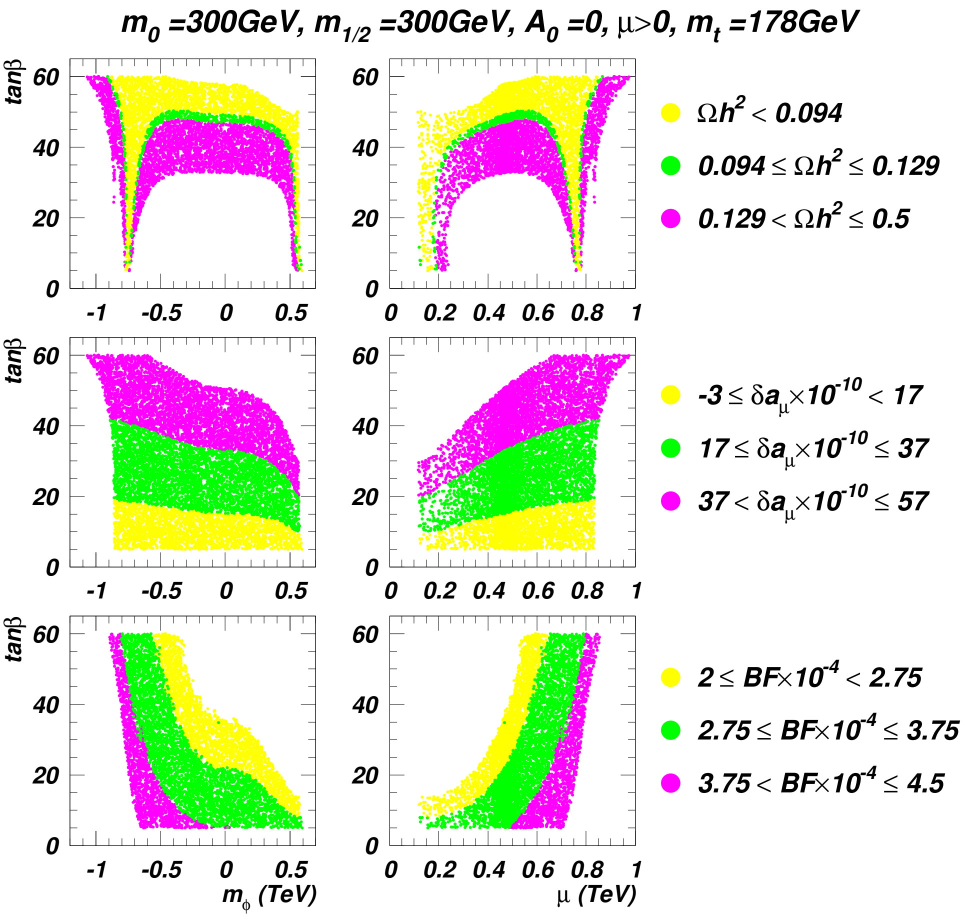

Figure 5: Ranges of Ωh^2, δa_μ and $BF(b \to s\gamma)$ for the NUHM1 models scanned in figure 4. If a parameter point falls outside the ranges shown, it is not plotted in this figure.

As we have already mentioned, there is still some debate on the range of the SM prediction for a_μ, as well as the MSSM prediction for $BF(b \to s\gamma)$. As a result, the χ^2 values in figure 4 should be interpreted with some care. To facilitate this, we show the ranges of Ωh^2, δa_μ and $BF(b \to s\gamma)$ for the same set of NUHM1 models as in figure 5. If a parameter set in figure 4 yields a value of these quantities that is outside the range shown, then the point is not plotted. From this plot we see why only the low $\tan\beta$ portion of the higgsino region at low μ gives low χ^2 in figure 4: at high $\tan\beta$, the $BF(b \to s\gamma)$ is quite high, while the value of Δa_μ is quite low. We see, however, a large swath of yellow with $\Omega_{CDM}h^2 < 0.094$ at large values of $\tan\beta$ in the upper frames of figure 5. This occurs because the A and H bosons become light and relatively wide, leading to a resonant enhancement (even off resonance) in the neutralino annihilation cross section and a corresponding reduction in the relic density. In this case, there must then be some other new physics that brings the CDM density up to the WMAP value.[2]

[2]We note that it is possible that this new physics associated with the non-LSP components of dark matter may also yield (possibly non-calculable) new contributions to both δa_μ and $BF(b \to s\gamma)$, so that

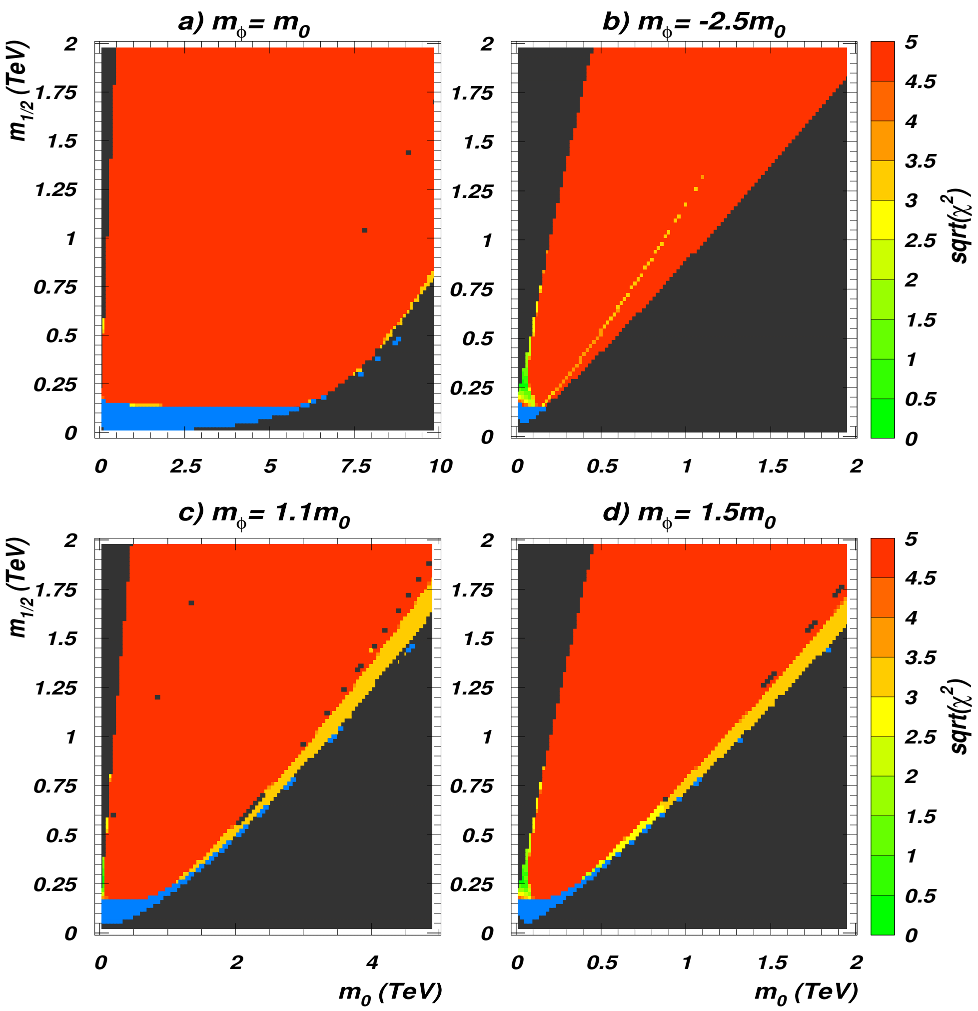

Figure 6: The $\sqrt{\chi^2}$ value in the m_0 vs. $m_{1/2}$ plane for $A_0 = 0$, $\tan\beta = 10$, $\mu > 0$ and $m_t = 178$ GeV. In frames *a)*, *b)*, *c)*, and *d)* we take $m_\phi/m_0 = 1$, -2.5, 1.1 and 1.5, respectively. The blue region is excluded by LEP2.

In figure 6, we show the m_0 vs. $m_{1/2}$ parameter space plane for the NUHM1 model, with $A_0 = 0$, $\tan\beta = 10$, $\mu > 0$, $m_t = 178\,\text{GeV}$ and *a)* $m_\phi = 0$ (mSUGRA case), *b)*, $m_\phi = -2.5m_0$, $m_\phi = 1.1m_0$ and $m_\phi = 1.5m_0$. The black regions are excluded by lack of REWSB (right hand side) and because the stau is the LSP on the left hand side. The blue shaded region is excluded by the LEP2 constraint that $m_{\widetilde{W}_1} < 103.5\,\text{GeV}$. The remaining parameter space is color coded according to the $\sqrt{\chi^2}$ value, and indeed we see that most of parameter space is excluded. The mSUGRA case of frame *a)* shows the HB/FP region at $m_0 \sim 8-10$ TeV, while the stau co-annihilation is squeezed against the left edge of the allowed parameter space. In frame *b)* for a large *negative* value of m_ϕ, we see that a narrow allowed region now cuts through the middle of the parameter plane. This is the

it may be premature to unequivocally exclude this parameter space region at large values of $\tan\beta$ because these quantities are not in agreement with their measured values.

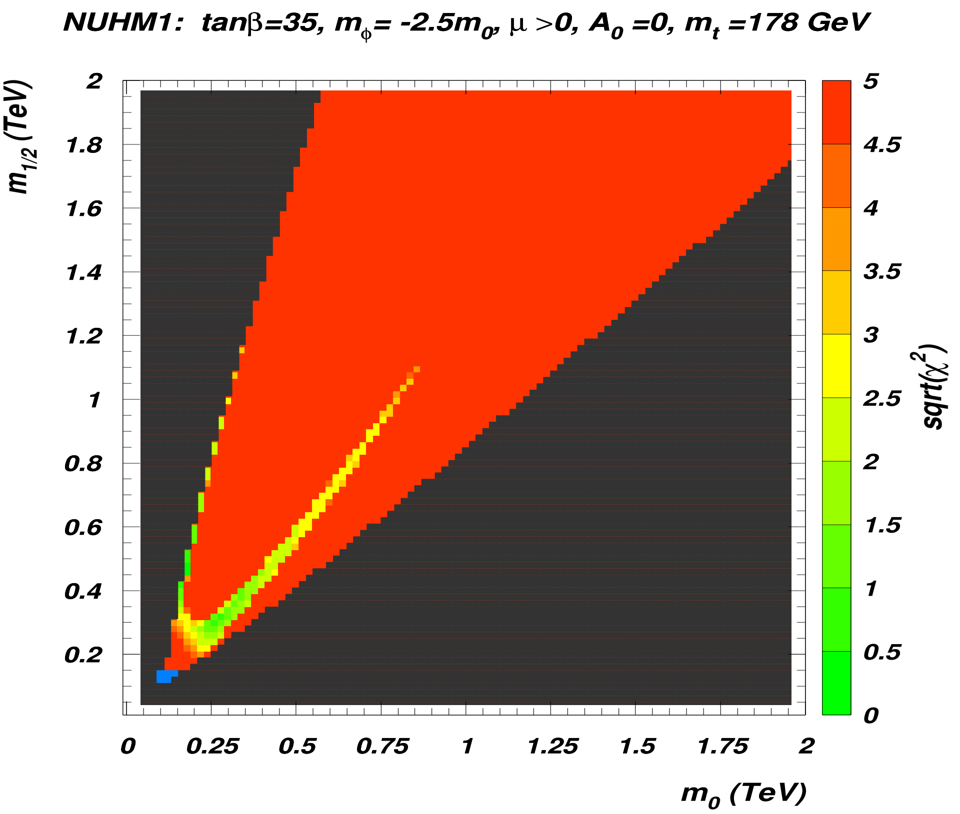

Figure 7: The $\sqrt{\chi^2}$ value in the m_0 vs. $m_{1/2}$ plane for $A_0 = 0$, $\tan\beta = 35$, $\mu > 0$ and $m_t = 178\,\text{GeV}$, with $m_\phi = -2.5m_0$. The blue region is excluded by LEP2.

A-annihilation funnel, which is much narrower than in the mSUGRA case at large $\tan\beta$, since now the A-width is relatively small: typically ~ 1 GeV. Note that the range of m_0 extends only to 2 TeV, since for larger values of m_0, $m_A^2 < 0$ and REWSB is violated. Since μ remains large, there is no higgsino LSP region along the right-hand edge of parameter space. In frame *c*) for $m_\phi = 1.1m_0$, we see that the m_0 parameter ranges only to 3 TeV, since now the right-hand side is excluded by $\mu^2 < 0$. This leads to a higgsino LSP region which is shaded yellow, which begins at $m_0 \sim 1\,\text{TeV}$ for low $m_{1/2}$, and explicitly shows that the higgsino LSP region can occur even for relatively light scalar masses. Frame *d*) for $m_\phi = 1.5m_0$ shows that the higgsino region has moved to even lower m_0 values, which are below 3 TeV even for $m_{1/2}$ as high as 2 TeV.

In figure 7, we show the $\sqrt{\chi^2}$ value in the m_0 vs. $m_{1/2}$ plane for $A_0 = 0$, $\tan\beta = 35$, $\mu > 0$, $m_\phi = -2.5m_0$ and $m_t = 178\,\text{GeV}$. This plane includes the region of lowest χ^2 value as indicated in figure 4. Here we see a well-defined A-annihilation funnel for the case of $\tan\beta = 35$, where the lower portion gives excellent agreement to the measured WMAP relic density, the branching fraction $BF(b \to s\gamma)$ and the muon anomalous magnetic moment Δa_μ. Excellent agreement is also obtained in this case for the stau co-annihilation region for $m_{1/2} \sim 350 - 600\,\text{GeV}$.

2.3 Dark matter detection: overview and methodology

Two major issues enter the evaluation of the prospects for neutralino dark matter detection and of assessing the relative effectiveness of the various direct and indirect techniques that have been proposed:

1. Since the detection rates critically depend on the dark matter halo profile of our own galaxy, and a wealth of observational data and theoretical constraints are available, the halo models one resorts to must be *consistent* with all information we have about the Milky Way. Moreover, since different detection techniques rely on the local dark matter density distribution and on the velocity distribution, a fair comparison among them may be carried out only provided the two distributions are *self-consistently* computed, not only locally, but throughout the whole halo.[3]

2. A comparison of the various techniques must rely on quantities which provide information on the relative strength of the expected signal with respect to the projected experimental sensitivity, taking into account the background. Toward this end, we use what have been dubbed *Visibility Ratios* (VR) [44−46, 25], which will be defined below for each experiment. A VR is simply a *signal-to-sensitivity* ratio: when VR>1, the signal calculated using a specified model is expected to be detectable over backgrounds with the particular experimental setup; in case VR<1, the signal will lie below the sensitivity of the considered detection facility. The locus of points at VR=1 outlines the actual *reach contour* of any particular detection technique. The relative magnitudes of the VR's for different dark matter search experiments provides a direct comparison between them [47].

As far as item 1. is concerned, we follow here the strategy outlined in ref. [44] (the reader is referred to ref. [48, 49, 45] for more details). Motivated by N-body simulations of hierarchical clustering in dark matter cosmologies, the starting point is to take into account the correlation between the virial mass of a given galaxy M_{vir} and its concentration parameter c_{vir} [50], and then to provide a description of the dynamics of the baryon infall and of its back-reaction onto the dark halo. Two extreme regimes have been outlined, the first one being motivated by a large angular momentum transfer between dark matter and baryons, while the second one by supposing that baryons settled in with no net transfer of angular momentum to the dark component.

In the first scenario, the central cusp in the dark matter halo, as seen in numerical simulations, is smoothed out by a significant heating of the cold particles [51], leading to a cored density distribution, which has been modeled by the so called *Burkert profile* [52],

$$\rho_B(r) = \frac{\rho_B^0}{(1 + r/a)\,(1 + (r/a)^2)}\,. \tag{2.12}$$

[3] We recall that, while the gamma ray flux from the galactic center only depends on the dark matter density in a very small, and poorly known region, the antimatter rates vary with the dark matter density in a more extended portion of the halo; finally the flux of neutrinos from neutralino annihilations in the sun and the direct detection rates essentially depend only on the density and velocity distributions of the dark halo within the solar system.

Here, the length scale parameter has been set to $a = 11.7$ kpc, while the normalization ρ_B^0 is adjusted to reproduce the local halo density at the Earth position to $\rho_B(r_0) = 0.34$ GeV cm^{-3} [48]. We refer to this model as to the *Burkert Halo Model.* It has been successfully tested against a large sample of rotation curves of spiral galaxies [53].

In the second scenario that we consider, baryon infall causes a progressive deepening of the gravitational potential well at the center of the galaxy, resulting in increasingly higher concentration of dark matter particles. In the circular orbit approximation [54, 55], this adiabatic contraction limit has been worked out starting from the N03 profile proposed in ref. [56]; the resulting spherical profile, which has no closed analytical form, roughly follows, in the inner galactic regions, the behavior of the profile proposed by Moore et al.,[57], approximately scaling as $r^{-1.5}$ in the innermost regions, and features a local dark matter density $\rho_{N03}(r_0) = 0.38$ GeV cm^{-3}. We dub this setup as the *Adiabatically Contracted N03 Halo Model.*

The parameters for both models have been chosen to reproduce a variety of dynamical information, ranging from the constraints stemming from the motion of stars in the sun's neighborhood, total mass estimates from the motion of the outer satellites, and consistency with the Milky Way rotation curve and measures of the optical depth toward the galactic bulge [48, 49]. Finally, the local velocity distributions of the two spherical profiles have been self-consistently computed using the formalism outlined in ref. [58], thus allowing for a reliable comparison between direct and indirect detection techniques. Both models have been included in the latest public release of the `DarkSUSY` package [24].

Turning to item 2., we begin by defining the Visibility Ratios (VR) mentioned above for each dark matter detection technique. For direct dark matter detection, in view of the fact that spin-dependent searches have been shown to be sensitive to scattering cross sections typically much larger than those predicted within the MSSM [45], we focus here only on spin-independent (SI) searches. The relevant quantity is the neutralino-proton SI scattering cross section, $\sigma^{\rm SI}_{\widetilde{Z}_1 p}$. The VR is simply defined as the ratio between the expected $\sigma^{\rm SI}_{\widetilde{Z}_1 p}$ from a given supersymmetric model and the corresponding experimental sensitivity $\sigma^{\rm SI}_{\rm exp}$ at the given neutralino mass, for the particular dark matter halo profile under consideration, taking into account the corresponding self-consistently computed local velocity distribution.[4] We consider here two benchmark direct detection experiments, namely CDMS-II [59] (stage-2 detectors) and the proposed XENON 1-ton facility (stage-3 detectors) [60, 61].

To assess the sensitivity of a km^2-size detector such as IceCube designed to detect high energy muons, we compute the expected muon flux from neutralino annihilations in the sun[5] above a threshold of 1 GeV. The low threshold was chosen to allow a comparison of the expected muon flux with the existing upper limits from the SuperKamiokande ex-

[4]The sensitivity of direct detection experiments may vary over more than two orders of magnitude for the typical range of neutralino masses in the MSSM. It also depends (less strongly) on the halo profile. In view of this sensitivity, we must be careful to use the corresponding value of $\sigma^{\rm SI}_{\rm exp}(m_{\widetilde{Z}_1})$ in the computation of the VR.

[5]We also evaluated the muon flux from the Earth, but always found far smaller fluxes than those expected from the sun.

periment (which indeed has a much lower energy threshold than IceCube) and to ensure that the model is not already excluded. The predicted muon flux is then compared with the sensitivity of IceCube. Since this detector has a higher energy threshold ~ 50 GeV, we corrected for the threshold mismatch using the corresponding projected sensitivities worked out in ref. [63]. We have checked that the projected maximal sensitivity to the muon flux obtained using this procedure is in good agreement with that obtained by integrating above the actual IceCube threshold. We also incorporated the dependence of the sensitivity on the soft (e.g. from neutralino annihilation to $b\bar{b}$) and hard (e.g. from annihilation to W^+W^-, Z^0Z^0 and $t\bar{t}$) neutrino spectra — the sensitivity being smaller in the case of the softer spectrum.

Turning to antimatter experiments, we compute the solar-modulated positron, antiproton and antideuteron fluxes, following the procedure outlined in ref. [44]. We calculate the neutralino annihilation rates to $\bar{p}$ and $\bar{n}$ using the `Pythia` 6.154 Monte Carlo code [64] as implemented in `DarkSUSY` [24], and then deduce the $\overline{D}$ yield using the prescription suggested in ref. [65]. The propagation of charged cosmic rays through the galactic magnetic fields is worked out through an effective two-dimensional diffusion model in the steady state approximation, while solar modulation effects were implemented through the analytical force-field approximation of Gleeson and Axford [66]. The solar modulation parameter Φ_F is computed from the proton cosmic-ray fluxes, and assumed to be charge-independent. The values of Φ_F we use for antiprotons and positrons refer to a putative average of the solar activity over the three years of data taking of the PAMELA experiment [67], which will be the first space-based experiment for antimatter searches.

For antideuterons we consider the reach of the proposed gaseous antiparticle spectrometer (GAPS) [68] proposed to be placed on a satellite orbiting around the Earth, and tuned to look for antideuterons in the very low kinetic energy interval from 0.1 to 0.4 GeV [68, 69]. In this energy interval, the estimated background is strongly suppressed [65, 70], and unambiguous evidence of even a single low energy antideuteron could be regarded as a positive search result. Since the experiment is expected to be launched close to the maximum of the solar cycle, we set the value of the solar modulation parameter Φ_F at the corresponding value. The resulting sensitivity of GAPS has been determined to be of the level of $2.6 \times 10^{-9}\mathrm{m}^{-2}\mathrm{sr}^{-1}\mathrm{GeV}^{-1}\mathrm{s}^{-1}$ [68]. The VR for antideuterons will then be given by the integrated $\overline{D}$ flux over the kinetic energy interval $0.1 < T_{\overline{D}} < 0.4\,\mathrm{GeV}$, divided by the GAPS sensitivity. In other words, the VR will give, in this case, the actual number of antideuterons expected to be detected by GAPS.

Regarding antiproton and positron fluxes, it was realized long ago that the low energy tails are considerably modified by solar modulation effects and, in the case of antiprotons, also by large secondary and tertiary backgrounds [71], so that low energy positrons and antiprotons cannot provide a clean test for new physics contributions. However, in view of the fact that novel space-based experiments will be able to extend the experimental sensitivity to these to the hundreds of GeV range, the best place to look for an antimatter signal from neutralino annihilations lies at the high energy end. Moreover, a distinctive signature is provided by the clean cutoff of the neutralino-induced antimatter flux corresponding to energies equal to the neutralino mass, provided this flux is large enough to be detectable. Nevertheless, in general, the energy spectra of antiparticles generally look quite featureless: aside from the fact that the antiparticles from neutralino annihilation sit on top of a featureless background, solar modulation and propagation effects also tend to wash away any features inherent to the spectrum. With some obvious exceptions, the antiparticle energy (or rather $E/m_{\widetilde{Z}_1}$) where the signal-to-background ratio is largest, is sensitive to the composition of the neutralino [72, 47]. Restricting attention to particular energy bin(s) may also be misleading because of large uncertainties from secondary and tertiary $\bar{p}$. A possible exception may be that of neutralinos mainly annihilating into gauge bosons, in which case one expects a bump in the positron spectrum at approximately half the neutralino mass [73]; this could be especially relevant for neutralinos in the HB/FP region.

To circumvent these problems, we adopt the statistical treatment of the antimatter yields introduced in ref. [44] (an analogous approach has been proposed for cosmic positron searches [74]). Motivated by the fact that the signal is much smaller than the background, we introduce a quantity which weighs its "statistical significance, summed over the energy bins",

$$I_\phi = \int_{T_{\rm min}}^{T_{\rm max}} \frac{(\phi_s(E))^2}{\phi_b(E)} {\rm d}E\,, \tag{2.13}$$

where $\phi_s(E)$ and $\phi_b(E)$ respectively represent the antimatter differential fluxes from neutralino annihilations and from the background at antiparticles' kinetic energy E, and $T_{\rm min,max}$ correspond to the antiparticle's maximal and minimal kinetic energies to which a given experiment is sensitive (in the case of the PAMELA experiment [67], $T^{e^+}_{\rm min} = 50$ MeV, $T^{e^+}_{\rm max} = 270\,{\rm GeV}$, $T^{\bar{p}}_{\rm min} = 80$ MeV and $T^{\bar{p}}_{\rm max} = 190\,{\rm GeV}$). We compute the primary component, ϕ_s, with the `DarkSUSY` package, interfaced with a subroutine implementing the diffusion and solar modulation models outlined above. The background flux ϕ_b has been calculated with the `Galprop` package [75], with the same parameter choices employed to compute the signal.

Given an experimental facility with a geometrical factor (acceptance) A and a total data-taking time T, it has been shown [44] that, in the limit of a large number of energy bins and of high precision secondary (i.e. background) flux determination, a SUSY model giving a primary antimatter flux ϕ_s can be discriminated at the 95% C.L. if

$$I_\phi(\phi_s) \cdot A \cdot T > (\chi^2)^{95\%}_{\rm n_b}\,, \tag{2.14}$$

where $(\chi^2)^{95\%}_{\rm n_b}$ stands for the 95% C.L. χ^2 with $\rm n_b$ degrees of freedom. For the PAMELA experiment, where $A = 24.5$ cm^2 sr, T=3 years and $\rm n_b \simeq 60$ we get the following discrimination condition [44]

$$I_\phi(\phi_s) > \frac{(\chi^2)^{95\%}_{\rm n_b}}{A \cdot T} \equiv I_\phi^{\rm 3y,\ PAMELA,\ 95\%} \simeq 3.2 \times 10^{-8}\ {\rm cm^{-2} sr^{-1} s^{-1}} \tag{2.15}$$

which is approximately valid for both positrons and antiprotons (though in the latter case the PAMELA experiment is expected to do slightly better). As a rule of thumb, the analogous quantity for AMS-02 should improve at least by one order of magnitude [73].

We therefore define as VR for antiprotons and for positrons the ratio

$$(\mathrm{VR})^{\bar{p},e^+} \equiv I_\phi^{\bar{p},e^+} / I_\phi^{\text{3y, PAMELA, 95\%}} . \tag{2.16}$$

Finally, the case for the gamma ray flux from the galactic center is plagued by large uncertainties on the very central structure of the Milky Way dark halo. Depending on various assumptions on the galactic models and on the physical cut-off in the inner part of our galaxy, there might be a spread of various orders of magnitude in the computation of the actual gamma-ray flux [76, 26]. This may be written as a product of a purely astrophysical quantity describing the propagation of the photons to the detector, and of a purely particle-physics quantity $\langle \sigma v \rangle$ [77] describing the source of these photons. The former reads,

$$\langle J(0) \rangle(\Delta\Omega) = \frac{1}{\Delta\Omega} \int_{\Delta\Omega} J(\psi) \mathrm{d}\Omega\,, \tag{2.17}$$

where

$$J(\psi) = \frac{1}{8.5 \text{ kpc}} \cdot \left(\frac{1}{0.3 \text{ GeV/cm}^3} \right)^2 \int_{\text{line of sight}} \rho^2(l) \mathrm{d}l(\psi)\,. \tag{2.18}$$

The attitude we take here is just to extrapolate the halo models we use in the $\rho(r \to 0)$ limit, and to compute the corresponding $\langle J(0) \rangle$ for the acceptance $\Delta\Omega$ of GLAST. What we find is $\langle J(0) \rangle = 7.85$ for the Burkert Halo Model, and $\langle J(0) \rangle = 1.55 \times 10^5$ for the Adiabatically Contracted N03 Halo Model.[6] We then compute the integrated gamma ray flux above a 1 GeV threshold, ϕ^γ, and define the corresponding VR as $\phi^\gamma/(1.5 \times 10^{-10}\ \mathrm{cm}^{-2}\mathrm{s}^{-1})$, the latter being the corresponding estimated sensitivity of the GLAST satellite [79].

2.4 Dark matter detection: the NUHM1 model

In figure 8 and 9 we show the VR's for the various experiments that we detailed in section 2.3, for two representative mSUGRA parameter choices: we fix $\tan\beta = 10$, $m_0 = 300\,\mathrm{GeV}$, $m_{1/2} = 300\,\mathrm{GeV}$ in figure 8, and $\tan\beta = 20$, $m_0 = 1000\,\mathrm{GeV}$, $m_{1/2} = 200\,\mathrm{GeV}$ in figure 9 (in both cases $A_0 = 0$, $\mathrm{sign}(\mu) > 0$ and $m_t = 178\,\mathrm{GeV}$) and show the results as a function of m_ϕ/m_0. The regions shaded in red are excluded by the LEP2 limits on the mass of the pseudoscalar Higgs boson m_A and on the mass of the lightest chargino. The green regions indicate, instead, parameter space regions where the neutralino relic abundance $\Omega_{\widetilde{Z}_1} h^2 < 0.13$, consistently with the WMAP 95% C.L. upper limit on the Cold Dark Matter abundance [80]: agreement with the central value of WMAP is obtained close to the boundary of this region. We remind the reader that a VR larger than unity means that the signal should be detectable in the particular dark matter detection channel. For definiteness, we adopt the conservative Burkert Halo Model. The results we show should be

[6] In the case of the Adiabatically Contracted halo model, this procedure is quite arbitrary, since different hypotheses on the dynamics of the central black hole formation might lead to very different predictions for the dark matter density in the center of the halo [55, 78]. Because there is an unconstrained extrapolation, essentially any flux may be possible.

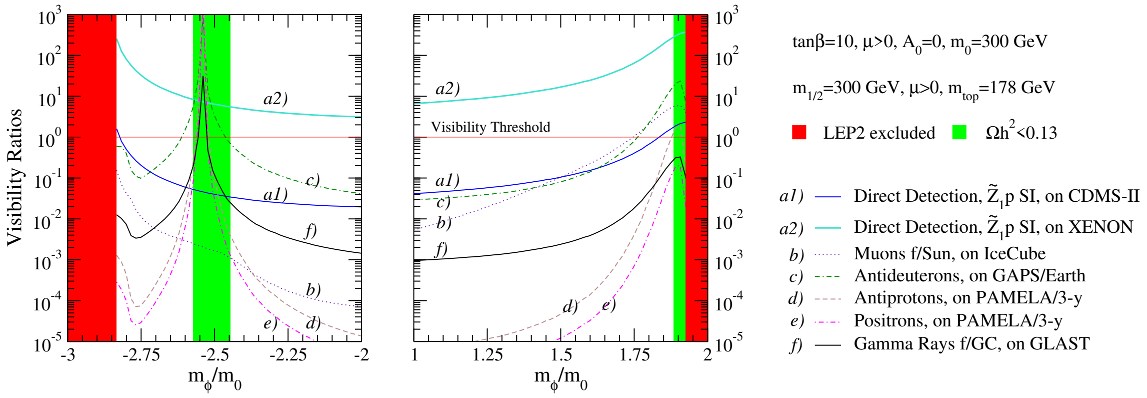

Figure 8: Dark matter detection Visibility Ratios (i.e. signal-to-projected-sensitivity ratios) for various direct and indirect techniques, as a function of the GUT scale non-universal Higgs mass parameter m_ϕ, for mSUGRA parameters $\tan\beta = 10$, $A_0 = 0$, sgn$\mu > 0$, $m_0 = 300\,\mathrm{GeV}$, $m_{1/2} = 300\,\mathrm{GeV}$, and setting $m_t = 178$ GeV. We take the dark matter distribution to be given by the cored Burkert Halo profile described in the text. A Visibility Ratio larger than one means that the signal will be detectable over background.

regarded as plausible *lower limits*, particularly as far as indirect rates are concerned since a cuspy inner dark halo would greatly enhance the dark matter detection rates [44, 76].[7]

We see, in figure 8, that for all values of m_ϕ the signal will be accessible to stage-3 direct detection facilities, like XENON 1-ton [60], while stage-2 detectors (such as CDMS-II [59]) will be able to probe only the HB/FP region, at large m_ϕ. The behavior of the direct detection VR's is readily understood. On the one hand, when m_ϕ takes large negative values, both m_A and the CP-even heavy Higgs boson mass m_H decrease; this leads to an enhancement of the t-channel H exchange in the neutralino-proton cross section (which scales as m_H^{-4}, assuming that $m_{A,H} \gg m_{\widetilde{Z}_1}$). On the other hand, when m_ϕ is large and positive, the higgsino fraction increases, and so does $\sigma^{\rm SI}_{\widetilde{Z}_1 p}$ since $\sigma^{\rm SI}_{\widetilde{Z}_1 p} \propto (Z_h Z_g)^2$, where $Z_{h,g}$ respectively denote the higgsino and bino fraction in the lightest neutralino. The same behavior for the direct detection VR applies to figure 9; here, once again, stage-3 detectors will be able to fully explore the parameter space, while only the focus point region will be discoverable at stage-2 facilities.

Turning to the neutralino-annihilations-induced flux of muons from the sun, we see that in both figures the resonant annihilation region gives rates which will be various orders of magnitude *below* the projected ultimate sensitivity of IceCube. This is because the neutralino capture rate in the sun (which mainly depends on the neutralino-proton *spin-dependent* scattering cross section) is not large enough: in contrast to the spin-independent cross section, in fact, the main contribution to the spin-dependent one comes from the Z exchange diagram, which is not enhanced by the smaller values of $m_{H,A}$. On the other hand, a larger higgsino fraction and annihilation cross section yields detectable rates at neutrino telescopes for the model considered in figure 8, at large m_ϕ; for the case addressed in figure 9 we see that the expected rates only lie less than one order of magnitude below

[7] This is explicitly illustrated for the NUHM2 Model in the next section.

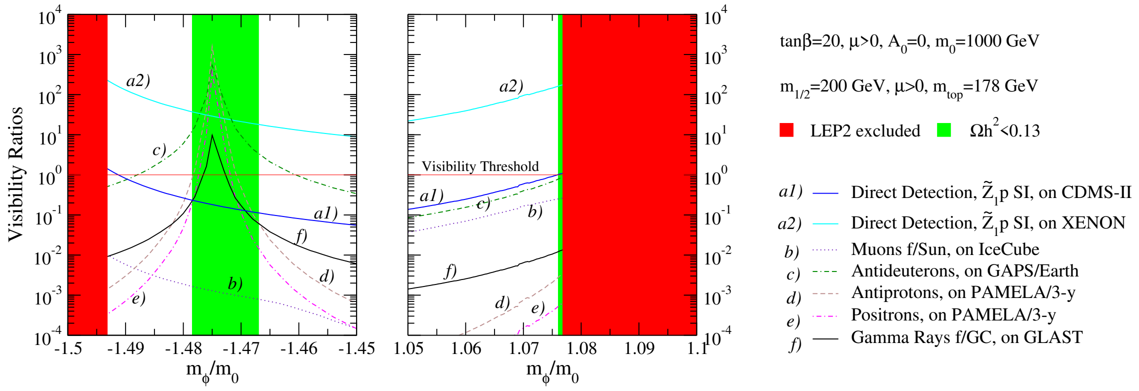

Figure 9: The same as figure 8, but with mSUGRA parameters $\tan\beta = 20$, $A_0 = 0$, $\mu > 0$, $m_0 = 1000\,\mathrm{GeV}$, $m_{1/2} = 200\,\mathrm{GeV}$.

the maximal sensitivity of IceCube. This is because for the smaller value of $m_{1/2}$, the neutralino LSP does not acquire a sufficiently large higgsino component all the way to the LEP2 limit.

As far as other indirect detection techniques are concerned, though we are here considering the conservative cored dark matter profile, the large neutralino pair annihilation rate $\langle\sigma v\rangle_0$ in the funnel region yields very large rates in all channels, peaked on the value of m_ϕ at which $m_A \simeq 2m_{\widetilde{Z}_1}$. A considerable enhancement is also seen in the HB/FP region. Despite this enhancement, antimatter detection rates might not be large enough to be discriminated against the background, especially in the case that we study in figure 9.

We should mention that for ranges of parameters that yield a thermal dark matter density smaller than the WMAP central value we do not correspondingly scale down the results in figure 8 and figure 9, as we would have to for any model where the remainder of the dark matter was composed of something other than the SUSY LSP (see e.g. ref. [81] and references therein). In this case, possible additional contributions from these other dark matter components would have to be included. We work here, instead, under the hypothesis that even within the low thermal relic density parameter ranges, the LSP is all of the dark matter, but that there is either additional *non-thermal production* [82], or *cosmological relic density enhancement*, as envisaged in ref. [83, 84] for quintessential cosmologies, in ref. [85] for Brans-Dicke-Jordan cosmologies, and in ref. [86, 87] for anisotropic cosmologies.

2.5 NUHM1 model: Collider searches for SUSY

While direct and indirect detection techniques that we have just discussed could establish the existence of dark matter, collider experiments would be needed to make the link with supersymmetry [88]. Collider expectations within the NUHM1 framework can differ from corresponding expectations within the well-studied mSUGRA model. In the following discussion, we highlight these differences confining our discussion to NUHM1 model parameter sets that satisfy the WMAP bound on $\Omega_{\widetilde{Z}_1} h^2$.

2.5.1 Fermilab Tevatron

The most promising avenue for a supersymmetry discovery at the Fermilab Tevatron in the case of gravity-mediated SUSY breaking models with gaugino mass unification is by the observation of trilepton signals from $p\bar{p} \to \widetilde{W}_1\widetilde{Z}_2X$ followed by $\widetilde{W}_1 \to \ell\nu_\ell\widetilde{Z}_1$ and $\widetilde{Z}_2 \to \ell\bar{\ell}\widetilde{Z}_1$ three body decays, where $\ell = e$ or μ [89, 90]. In the case of the NUHM1 model where m_ϕ is taken to have negative values so that neutralinos annihilate via the A and H poles, the only effect on the gaugino/higgsino sector is that the magnitude of the μ parameter increases. As a result, the HB/FP region of small $|\mu|$ is absent in frame *b*) of figure 10, so that unlike the case of mSUGRA [90], probing large values of m_0 and $m_{1/2}$ via this channel will not be possible. Alternatively, if m_ϕ is taken to be large compared to m_0 so that $|\mu|$ is small, then chargino and neutralino masses can become lighter, which may increase production cross sections. Furthermore, the $m_{\widetilde{Z}_2} - m_{\widetilde{Z}_1}$ mass gap will diminish, which can close "spoiler" decay modes such as $\widetilde{Z}_2 \to \widetilde{Z}_1 h$, so that the necessary three-body neutralino decays are more likely to be in effect, and because $\tan\beta$ is not necessarily large, we do not expect events with tau leptons to dominate at the expense of e and μ events. Thus, in the large m_ϕ region, we expect improved prospects for clean trilepton signals. Detailed simulation would of course be necessary to draw definitive conclusions.

2.5.2 CERN LHC

The CERN LHC is expected to begin operation in 2007 with pp collisions at $\sqrt{s} = 14\,\mathrm{TeV}$. In most regions of parameter space of gravity-mediated SUSY breaking models, gluino and squark pair production is expected to be the dominant source of sparticles at the LHC. Since the values of m_0 and $m_{1/2}$ determine for the most part the magnitudes of the squark and gluino masses, we expect sparticle production rates in the NUHM1 model to be similar to those in the mSUGRA model for the same model parameter choices. The reach of the CERN LHC in the case of the mSUGRA model has recently been re-evaluated in the m_0 vs. $m_{1/2}$ plane for various $\tan\beta$ values, and assuming 100 fb^{-1} of integrated luminosity in ref. [91]. We display this reach contour on frame *a*) of figure 10 where as in figure 6 *a*) we take $A_0 = 0$, $\tan\beta = 10$ and $m_\phi = m_0$ (mSUGRA case). We also show the WMAP allowed region ($\Omega_{\widetilde{Z}_1}h^2 < 0.13$) as the one shaded in green. The low m_0 portion of the reach contour extends to $m_{1/2} \sim 1.3\,\mathrm{TeV}$, and corresponds roughly to $m_{\tilde{q}} \sim m_{\tilde{g}} \sim 3\,\mathrm{TeV}$. The high m_0 portion of the reach contour extends to $m_{1/2} \sim 0.7\,\mathrm{TeV}$, and corresponds to $m_{\tilde{g}} \sim 1.8\,\mathrm{TeV}$, while squarks are in the multi-TeV range, and essentially decoupled. Note that in this frame the parameter m_0 ranges all the way to 10 TeV.

In frame *b*), with $m_\phi = -2.5m_0$, a much smaller range of m_0 is allowed, and the plot only extends to $m_0 = 2\,\mathrm{TeV}$. Since the reach is mainly determined by the values of the squark and gluino masses, we adapt the reach contours from ref. [91] to this non-mSUGRA case. Here, it is seen that the LHC reach covers almost all of the allowed A annihilation funnel. In frames *c*) and *d*), we show the cases for $m_\phi = 1.1m_0$ and $1.5m_0$, respectively. Here, the HB/FP type region re-emerges, but at much lower m_0 values, as discussed in section 2.2. The LHC reach is shown to cover all of the bulk and stau co-annihilation regions, but only a part of the higgsino annihilation (HB/FP) region.

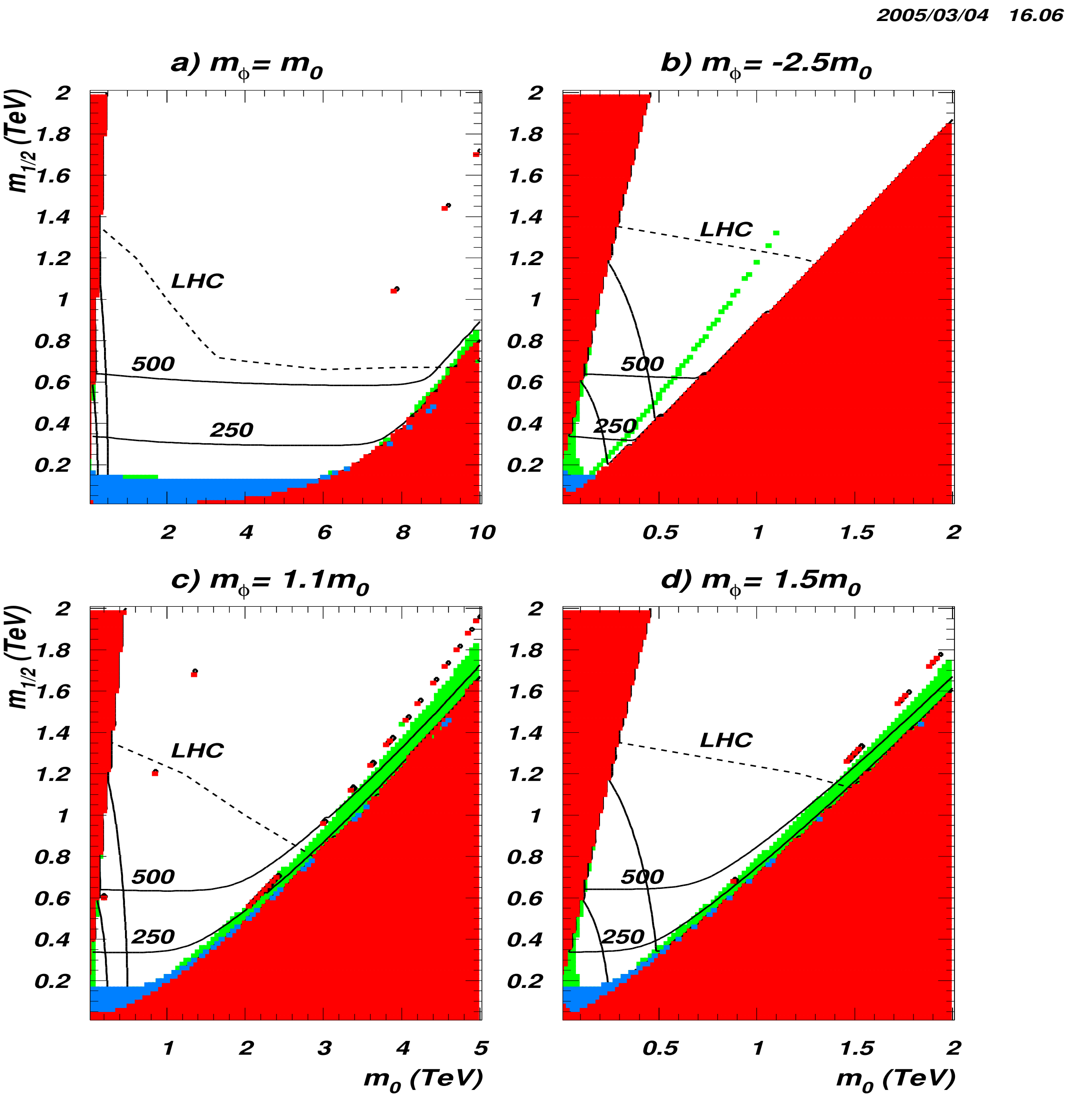

Figure 10: Approximate projections for the reach of the CERN LHC (100 fb^{-1}) and ILC in the NUHM1 model in the m_0 vs. $m_{1/2}$ plane for $\tan\beta = 10$, $A_0 = 0$, $\mu > 0$ and $m_t = 178\,\mathrm{GeV}$, for various choices of m_ϕ/m_0. The regions shaded in green are consistent with the WMAP constraint $\Omega h^2 < 0.13$, while those shaded in red and blue are respectively excluded by theoretical and experimental constraints discussed in the text.

While we expect a similar reach of the LHC (in terms of $m_{\tilde{q}}$ and $m_{\tilde{g}}$ parameters) to be found in both the mSUGRA and NUHM1 models, the detailed gluino and squark cascade decays will change, as will the expected SUSY Higgs signals. To exemplify this, we list in table 1 three model points. The first corresponds to mSUGRA for $m_0 = m_{1/2} = 300\,\mathrm{GeV}$, $A_0 = 0$, $\tan\beta = 10$, $\mu > 0$ and $m_t = 178$ GeV. We list a variety of sparticle and Higgs boson masses, along with $\Omega_{\widetilde{Z}_1} h^2$, $BF(b \to s\gamma)$ and Δa_μ. The second and third points listed, NUHM1a and NUHM1b, correspond to the same mSUGRA model parameters, but

JHEP07(2005)065

parameter	mSUGRA	NUHM1a	NUHM1b
m_ϕ	300	-735	550
μ	409.2	754.0	180.6
$m_{\tilde{g}}$	732.9	736.2	732.0
$m_{\tilde{u}_L}$	720.9	720.5	722.4
$m_{\tilde{t}_1}$	523.4	632.4	481.0
$m_{\tilde{b}_1}$	650.0	691.6	631.0
$m_{\tilde{e}_L}$	364.7	366.4	364.5
$m_{\tilde{e}_R}$	322.8	322.1	323.0
$m_{\widetilde{W}_2}$	432.9	759.6	280.3
$m_{\widetilde{W}_1}$	223.9	236.2	150.2
$m_{\widetilde{Z}_4}$	433.7	759.5	283.4
$m_{\widetilde{Z}_3}$	414.8	752.0	190.3
$m_{\widetilde{Z}_2}$	223.7	235.8	160.7
$m_{\widetilde{Z}_1}$	117.0	118.7	102.7
m_A	538.6	265.0	603.8
m_{H^+}	548.0	278.2	613.0
m_h	115.7	116.1	115.3
$\Omega_{\widetilde{Z}_1}h^2$	1.2	0.12	0.11
$BF(b \to s\gamma)$	3.2×10^{-4}	4.7×10^{-4}	2.5×10^{-4}
Δa_μ	12.1×10^{-10}	9.4×10^{-10}	17.4×10^{-10}

Table 1: Masses and parameters in GeV units for mSUGRA and two NUHM1 models, where $m_0 = m_{1/2} = 300\,\mathrm{GeV}$, $A_0 = 0$, $\tan\beta = 10$ and $m_t = 178\,\mathrm{GeV}$.

with $m_\phi = -735\,\mathrm{GeV}$ and $550\,\mathrm{GeV}$, respectively. The mSUGRA case can be seen to have $\Omega_{\widetilde{Z}_1}h^2 = 1.2$, and is thus strongly excluded by WMAP data, while the two NUHM1 points have $\Omega_{\widetilde{Z}_1}h^2 \sim 0.11$, and give the correct amount of CDM in the universe. The NUHM1a point has a similar spectrum of sparticles compared to the mSUGRA case, although the heavier chargino and neutralinos have increased masses due to the larger value of the μ parameter. The main difference is that the heavier Higgs bosons are relatively light in the NUHM1a case, and can be accessible to LHC searches as well as at a TeV-scale linear collider. In the case of mSUGRA, only the lightest Higgs h will be detectable at the LHC via direct h production followed by $h \to \gamma\gamma$ decay, or via $t\bar{t}h$ or Wh production, followed by $h \to b\bar{b}$ decay. The h should also be observable in the sparticle cascade decays [93]. In the NUHM1a case with $m_A = 265\,\mathrm{GeV}$, the H and A Higgs bosons are much lighter, and should be detectable via direct H and A production followed by $H,\ A \to \tau\bar{\tau}$ decay [92]. The reaction $gb \to tH^+$ followed by $H^+ \to \tau^+\nu_\tau$ appears to be on the edge of observability. If $\tan\beta$ is increased to values beyond 15, then $H,\ A \to \mu^+\mu^-$ [94] should become visible.

In the case of NUHM1b, m_ϕ is taken large enough that μ becomes small, 180.6 GeV, and the lightest neutralino develops a sufficient higgsino component to respect the WMAP dark matter constraint. The low μ value pulls the various heavier chargino and neutralino masses to low values ranging from $190-283\,\mathrm{GeV}$. In this case, gluinos and squarks will be copiously produced at the LHC. Gluinos dominantly decay via two body modes to $\tilde{t}_1 t$ (BF $\simeq 49\%$) and $\tilde{b}_{1,2} b$ (BF $\simeq 39\%$). The lighter stop decays via $\tilde{t}_1 \to b\widetilde{W}_{1,2}$ (53%), $\tilde{t}_1 \to t\widetilde{Z}_3$ (25%), while $\tilde{b}_1(\tilde{b}_2)$ mainly decays to the two charginos (roughly democratically to all charginos and neutralinos). The left squarks decay mainly to both charginos and to $\widetilde{Z}_{1,2}$, while $\tilde{q}_R$ mainly decays via $\tilde{q}_R \to \widetilde{Z}_{1,2}$. The lighter chargino decays via three body decays with branching fractions corresponding to those of the virtual W. On the other hand, $\widetilde{Z}_{2,3}$ decays via three body decays with the leptonic branching fraction $BF(\widetilde{Z}_{2(3)} \to \ell\bar{\ell}\widetilde{Z}_1) \simeq 1.5(3)\%$ per lepton family. Finally the heavier chargino mainly decays via $\widetilde{W}_2 \to W\widetilde{Z}_2, \widetilde{W}_1 Z$, while $\widetilde{Z}_4 \to \widetilde{W}_1 W$. It is clear that the LHC will be awash in SUSY events, with gluino and squark production being the dominant production mechanism. In this scenario, the total SUSY cross section is almost 10^4 fb, so that even at the low luminosity, we should expect $\sim 100,000$ SUSY events annually. Moreover, from our discussion of the sparticle decay patterns, we see that *all* the charginos and neutralinos should be accessible via cascade decays of gluinos and squarks, as envisioned in ref. [95]. It would be extremely interesting to perform a detailed study of just how much information about the SUSY spectrum the LHC data would be able to provide in this case. While detailed simulation would be necessary before definitive statements can be made, it is plausible that analyses along the lines carried out in ref. [96] may yield information about a large part of the sparticle spectrum, and provide a real connection between collider experiments and dark matter searches.

2.5.3 Linear e^+e^- collider

The reach of a $\sqrt{s} = 0.5$ and 1 TeV international linear e^+e^- collider (ILC) for supersymmetry has been evaluated with special attention on the HB/FP region in ref. [97] in the case of the mSUGRA model. In this study it was shown that the reach contours in the m_0 vs. $m_{1/2}$ plane are determined mainly via the reach for sleptons pairs, the reach for chargino pairs, and partly by the reach in $\widetilde{Z}_1\widetilde{Z}_2$ production. There is also a significant reach for the Higgs bosons H, A and H^+ in the large $\tan\beta$ case. The striking result of ref. [97] was that in the WMAP allowed HB/FP region, $|\mu|$ becomes small and charginos become light, the reach of the ILC extends beyond that of the LHC. In the HB/FP region of the mSUGRA model, squarks are in the multi-TeV regime, and effectively not produced at the LHC. The signal at the LHC becomes rate limited for $m_{\tilde{g}} \gtrsim 1.8$ TeV.

In figure 10, we also show contours of $m_{\widetilde{W}_1}$ and $\min(m_{\tilde{e}_L,\tilde{e}_R}) = 250$ GeV and 500 GeV: since signals from chargino and selectron pairs can be probed at an e^+e^- linear collider nearly up to the kinematic limit for their production, these contours follow the boundary of the region that would be probed at the ILC. Frame *a*) shows the mSUGRA case where an ILC would have an extended reach in the HB/FP region around $m_0 \sim 8 - 10\,\mathrm{TeV}$. In frame *b*) where the DM-allowed regions consist only of the A-funnel and stau-co-annihilation corridor, the ILC reach is well below that of the LHC. In frames *c*) and *d*), where $m_\phi > m_0$, the HB/FP region has moved to much lower values of m_0. However, in these regions, again μ becomes small so that charginos become light, and the ILC reach for $\widetilde{W}_1^+\widetilde{W}_1^-$ pairs may exceed the reach of the LHC along the right-hand edge of parameter space, even in frame *d*) where squarks are comparatively light.

Concerning the specific SUSY models shown in table 1, in the case of the mSUGRA model, the ILC operating at $\sqrt{s} = 500\,\text{GeV}$ would see of course Zh production, but also $\widetilde{W}_1^+\widetilde{W}_1^-$ and $\widetilde{Z}_1\widetilde{Z}_2$ production. The cross section for the latter process is ~ 200 fb, and since $\widetilde{Z}_2 \to \widetilde{Z}_1 Z^0$ essentially all the time, the end points of the energy distribution of Z^0 should yield the values of $\widetilde{Z}_1$ and $\widetilde{Z}_2$ masses to good precision. This is, of course, over and above $m_{\widetilde{W}_1}$ which can be determined as usual. In the NUHM1a model, where now the MSSM Higgs sector becomes light, H^0Z^0 and A^0h production will also be possible, allowing a detailed study of the Higgs sector and possibly a good determination of $\tan\beta$ [98]. If the ILC energy is increased somewhat above 500 GeV, then H^+H^- also becomes accessible to study. For the NUHM1b model, the Higgs bosons again become heavy, but the various heavier charginos and neutralinos become light. In this case, the final states $\widetilde{Z}_1\widetilde{Z}_3$, $\widetilde{Z}_1\widetilde{Z}_4$, $\widetilde{Z}_2\widetilde{Z}_2$, $\widetilde{Z}_2\widetilde{Z}_3$, $\widetilde{Z}_2\widetilde{Z}_4$ and even $\widetilde{Z}_3\widetilde{Z}_4$ as well as $\widetilde{W}_1^\pm\widetilde{W}_2^\mp$ are kinematically accessible. Thus, a whole host of heavier chargino/neutralino states would be available for study. If the ILC energy is increased to 1 TeV, then as in the mSUGRA case, the various slepton pair production as well as $\widetilde{W}_1\widetilde{W}_2$ pair production would be available for study and SUSY spectroscopy would become a reality. Moreover, the heavier Higgs bosons A, H and $H^\pm$ which now have substantial branching fractions to charginos and neutralinos, will also be accessible to study.

3. NUHM2 model

3.1 Overview

The NUHM2 model is characterized by two additional parameters beyond the mSUGRA set. The two new parameters may be taken to be the GUT scale values of $m_{H_u}^2$ and $m_{H_d}^2$, where these parameters may take on both positive and negative values. The model parameter space is given by

$$m_0,\ m_{H_u}^2,\ m_{H_d}^2,\ m_{1/2},\ A_0,\ \tan\beta,\ \text{sign}(\mu)\,. \tag{3.1}$$

We remind the reader that at tree level the Higgs scalar potential is completely specified by $m_{H_u}^2$, $m_{H_d}^2$, μ^2 and the parameter $B\mu$. The two minimization conditions allow us to trade two of $m_{H_u}^2$, $m_{H_d}^2$, μ^2 and $B\mu$ in favor of $tan\beta$ and M_Z^2, while a third may be traded for the CP odd Higgs scalar mass m_A. In (3.1) above, μ^2 and $B\mu$ have been traded for $\tan\beta$ and M_Z^2, leaving the sign of μ (which enters via the chargino and neutralino mass matrices) undetermined. Alternatively, in the NUHM2 model, we could have eliminated $m_{H_u}^2$, $m_{H_d}^2$ and $B\mu$ leaving $\tan\beta$ together with the weak scale values of μ and m_A as input parameters. Thus, the set

$$m_0,\ \mu,\ m_A,\ m_{1/2},\ A_0,\ \tan\beta\,, \tag{3.2}$$

where μ, m_A and $\tan\beta$ are input as weak scale values, while the remaining parameters are GUT scale values, provides an alternative parametrization of the NUHM2 model. In mSUGRA, we have two additional constraints, $m_{H_u}^2 = m_{H_d}^2 = m_0^2$, on the scalar potential and the values of μ^2 and m_A are determined.

JHEP07(2005)065

We have upgraded Isajet v7.72 to allow not only the input of negative Higgs squared masses at the GUT scale, but also to accommodate the second of these parameter sets with weak scale values of μ and m_A as inputs, using the non-universal SUGRA (NUSUG) input parameters [23]. The NUHM1 and NUHM2 models in Isajet incorporate REWSB using the RG improved one-loop effective potential, minimized at an optimal scale $Q = \sqrt{m_{\tilde{t}_L} m_{\tilde{t}_R}}$ to account for dominant two-loop contributions.

An important aspect of the NUHM2 model is that RG running of soft masses is in general modified by the presence of a non-zero S term in Eq. (2.8). The quantity S, which in the NUHM2 model is given by $S = m_{H_u}^2 - m_{H_d}^2$, enters the third generation soft scalar squared mass RGEs as,

$$\frac{dm_{Q_3}^2}{dt} = \frac{2}{16\pi^2}\left(-\frac{1}{15}g_1^2 M_1^2 - 3g_2^2 M_2^2 - \frac{16}{3}g_3^2 M_3^2 + \frac{1}{10}g_1^2 S + f_t^2 X_t + f_b^2 X_b\right), \tag{3.3}$$

$$\frac{dm_{\tilde{t}_R}^2}{dt} = \frac{2}{16\pi^2}\left(-\frac{16}{15}g_1^2 M_1^2 - \frac{16}{3}g_3^2 M_3^2 - \frac{2}{5}g_1^2 S + 2f_t^2 X_t\right), \tag{3.4}$$

$$\frac{dm_{\tilde{b}_R}^2}{dt} = \frac{2}{16\pi^2}\left(-\frac{4}{15}g_1^2 M_1^2 - \frac{16}{3}g_3^2 M_3^2 + \frac{1}{5}g_1^2 S + 2f_b^2 X_b\right), \tag{3.5}$$

$$\frac{dm_{L_3}^2}{dt} = \frac{2}{16\pi^2}\left(-\frac{3}{5}g_1^2 M_1^2 - 3g_2^2 M_2^2 - \frac{3}{10}g_1^2 S + f_\tau^2 X_\tau\right), \tag{3.6}$$

$$\frac{dm_{\tilde{\tau}_R}^2}{dt} = \frac{2}{16\pi^2}\left(-\frac{12}{5}g_1^2 M_1^2 + \frac{3}{5}g_1^2 S + 2f_\tau^2 X_\tau\right). \tag{3.7}$$

The first and second generation soft mass RGEs are similar, but with negligible Yukawa coupling contributions. The Higgs boson soft mass RGEs are as given by (2.3) and (2.4). The coefficients of the S terms are all proportional to the weak hypercharge assignments, so that this term provides a source of intra-generational mass splitting. When S is large and positive (i.e. , when $m_{H_u}^2 > m_{H_d}^2$), the mass parameters for $\tilde{\tau}_R$, $\tilde{e}_R$ and $\tilde{\mu}_R$ are the most suppressed, while those for $\tilde{q}_R$ and $\tilde{\ell}_L$ are enhanced. If S is large and negative, the situation is exactly reversed. For large values of $|S|$, the sfermion mass ordering as well as mixing patterns of third generation sfermions may be altered from mSUGRA expectations, or for that matter expectations in many other models of sparticle masses. For instance, it is possible that $m_{\tilde{\ell}_L} < m_{\tilde{\ell}_R}$; moreover, while the lighter stau is usually expected to be dominantly $\tilde{\tau}_R$ in most models, this may no longer be the case in the NUHM2 model.

As a simple illustration of how the spectrum of the NUHM2 model varies with the Higgs boson mass parameters, in figure 11 we show the physical masses of various sparticles versus $\Delta m_H \equiv m_0 - \mathrm{sign}(m_{H_u}^2)\cdot\sqrt{|m_{H_u}^2|} = \mathrm{sign}(m_{H_d}^2)\cdot\sqrt{|m_{H_d}^2|} - m_0$. This is a one parameter section of the NUHM2 parameter space we call the Higgs splitting (HS) model, with $\Delta m_H = 0$ corresponding to the mSUGRA model. Large positive Δm_H gives rise to a large *negative* S, and vice versa. In our example, we take $m_0 = m_{1/2} = 300\,\mathrm{GeV}$, with $A_0 = 0$, $\tan\beta = 10$ and $\mu > 0$. As Δm_H increases, we see that in the first generation, the $\tilde{e}_R$, $\tilde{d}_R$ and $\tilde{u}_L$ masses all increase, while $\tilde{e}_L$ and $\tilde{u}_R$ masses decrease. In mSUGRA, $m_{\tilde{e}_R}$ is always less than $m_{\tilde{e}_L}$; in NUHM2 models, this mass ordering may be reversed. At

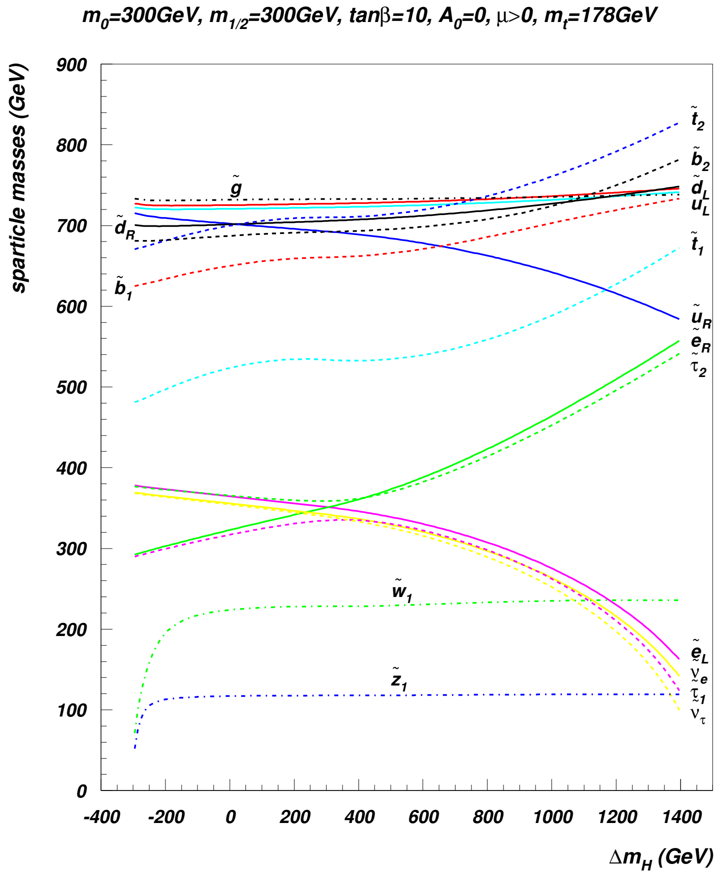

Figure 11: Variation in sparticle masses versus Δm_H in the NUHM2 model, for $m_0 = 300\,\text{GeV}$, $m_{1/2} = 300\,\text{GeV}$, $A_0 = 0$, $\tan\beta = 10$, $\mu > 0$ and $m_t = 178\,\text{GeV}$.

the highest allowed values of Δm_H, the $\tilde{\nu}_\tau$ and $\tilde{\tau}_1$ mass values become light (and $\tilde{\tau}_1$ is then dominantly $\tilde{\tau}_L$), enhancing t-channel $\widetilde{Z}_1\widetilde{Z}_1 \to \nu_\tau\bar{\nu}_\tau,\ e^+e^-,\ \nu_\mu\bar{\nu}_\mu,\ \mu^+\mu^-$ annihilation in the early universe, which lowers the relic density to within the WMAP bound. When $m_{\tilde{\nu}_\tau},\ m_{\tilde{\tau}_1} \simeq m_{\widetilde{Z}_1}$, then co-annihilation reduces the relic density even further.

Some aspects of NUHM2 phenomenology as a function of Δm_H are illustrated in figure 12. In frame *a*) we show the values of μ, m_A and $m_{\widetilde{Z}_1}$ versus Δm_H. For negative values of Δm_H, both μ and m_A are small, and we have a region of higgsino and (possibly) A-funnel annihilation. For Δm_H large and positive, the relic density, shown in frame *b*), drops because left sleptons and sneutrinos become very light. The value of $BF(b \to s\gamma)$ and Δa_μ are also shown in frames *c*) and *d*). These rise for negative values of Δm_H because the charged Higgs bosons and the lighter charginos and neutralinos become very light with the -inos developing significant higgsino components.

In figure 13 we show again the variation in sparticle masses with Δm_H, but this time for $m_0 = 1450\,\text{GeV}$, $m_{1/2}$=300 GeV, $A_0 = 0$, $\tan\beta = 10$ and $\mu > 0$. In this case, the large scalar masses yield a large S term in the RGEs, and the hypercharge enhancement/suppression is accentuated. We see, as noted in ref. [41] for Yukawa unified models, that the $\tilde{u}_R$ and

JHEP07(2005)065

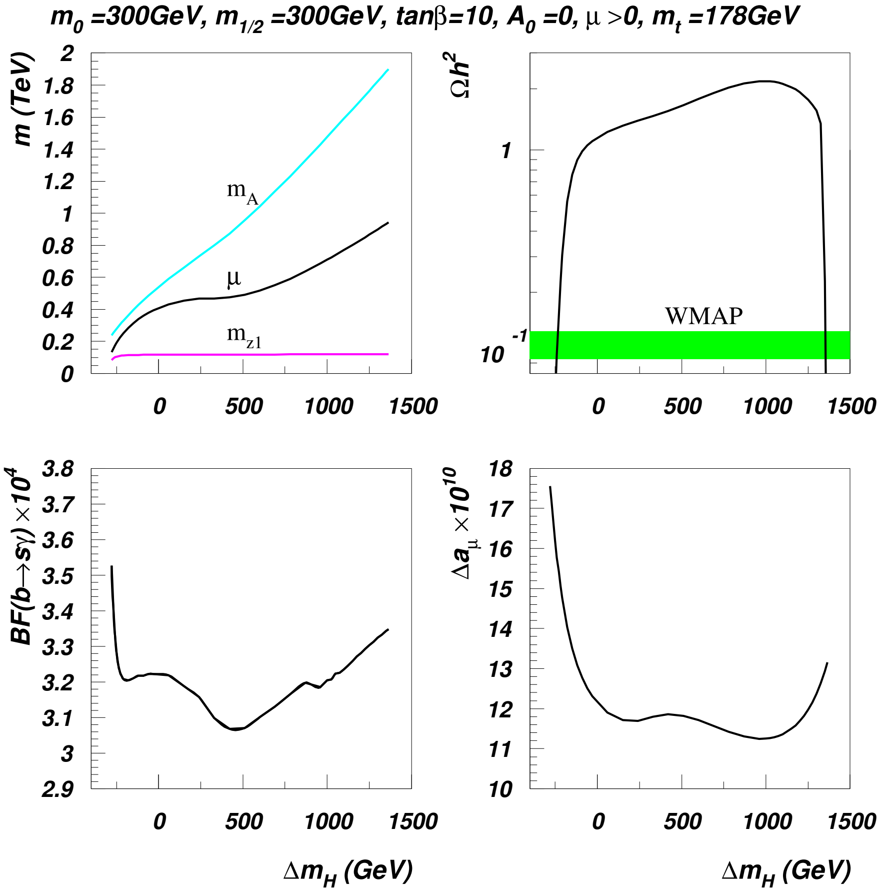

Figure 12: Variation in *a)* m_A, μ and $m_{\widetilde{Z}_1}$, *b)* $\Omega_{\widetilde{Z}_1}h^2$, *c)* $BF(b \to s\gamma)$ and *d)* Δa_μ versus $\Delta m_H \equiv (m_{H_d} - m_{H_u})/2$ in the NUHM2 model, for $m_0 = 300\,\mathrm{GeV}$, $m_{1/2} = 300\,\mathrm{GeV}$, $A_0 = 0$, $\tan\beta = 10$, $\mu > 0$ and $m_t = 178\,\mathrm{GeV}$.

$\tilde{c}_R$ squarks are driven to very low mass values as Δm_H increases. At the high end of the Δm_H range, they become the lightest squarks, even lighter than the $\tilde{t}_1$. The large Δm_H parameter space ends when $\tilde{u}_R$ becomes a charged/colored LSP, in violation of restrictions forbidding such cosmological relics. We also see that as Δm_H increases, the $\tilde{t}_1$ mass at first increases, then decreases, then increases again. The initial increase is because as Δm_H increases, X_t decreases, leading to reduced Yukawa coupling suppression of the soft SUSY breaking mass parameters of top squarks. For still larger values of Δm_H, the S term grows and leads to a suppression of the $\tilde{t}_R$, and hence $\tilde{t}_1$ mass. Finally, as Δm_H is increased even more, the X_t term becomes large and *negative*, and again resulting in an increase in the top squark soft masses. We have checked that throughout this range of Δm_H, the lighter top squark remains predominantly right-handed.

In figure 14, we show the same frames as in figure 12, but now for the $m_0 = 1450\,\mathrm{GeV}$ case. At low Δm_H values, again μ gets to be small, so that the neutralino becomes higgsino-like leading to efficient annihilation in the early universe. At very large Δm_H values, the relic density is again in accord with the WMAP analysis — this time because

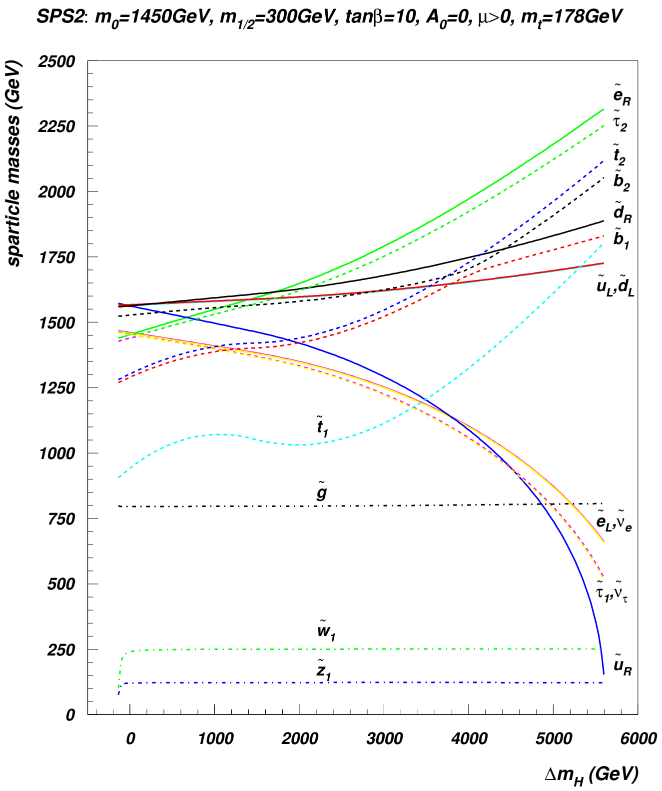

Figure 13: Variation of sparticle masses versus Δm_H defined in the text for the NUHM2 model, with $m_0 = 1450\,\mathrm{GeV}$, $m_{1/2} = 300\,\mathrm{GeV}$, $A_0 = 0$, $\tan\beta = 10$, $\mu > 0$ and $m_t = 178\,\mathrm{GeV}$.

the squarks become so light that neutralinos can efficiently annihilate via $\widetilde{Z}_1\widetilde{Z}_1 \to u\bar{u},\ c\bar{c}$ processes occurring via t-channel $\tilde{u}_R$ and $\tilde{c}_R$ exchange. Furthermore, if $m_{\tilde{u}_R}$ and $m_{\tilde{c}_R}$ are in the 100-200 GeV range, they may be accessible to Tevatron searches! The light squarks also lead to a greatly enhanced neutralino-proton scattering rate, and hence to large rates for direct detection of relic neutralinos [41]. There is a small enhancement in Δa_μ at low Δm_H where charginos and neutralinos become light and higgsino-like, leading to larger chargino-sneutrino and neutralino-smuon loop contributions in the evaluation of $(g-2)_\mu$ [43].

3.2 NUHM2 model: parameter space

Our first display of the parameter space of the NUHM2 model is in figure 15, where we show the $\mathrm{sign}(m_{H_u}^2)\cdot\sqrt{|m_{H_u}^2|}$ vs. $\mathrm{sign}(m_{H_d}^2\cdot\sqrt{|m_{H_d}^2|}$ plane for $m_0 = m_{1/2} = 300\,\mathrm{GeV}$, with $A_0 = 0$, $\tan\beta = 10$, $\mu > 0$ and $m_t = 178\,\mathrm{GeV}$. In frame *a*) we show the allowed parameter space as the white region, while theoretically excluded parameter choices are red. The region to the right is excluded because $\mu^2 < 0$. In the red region at the bottom, $m_A^2 < 0$, while in that on the top, $\widetilde{Z}_1$ is not the LSP.

The blue region is allowed theoretically, but here, $|\mu|$ dives to small values yielding $m_{\widetilde{W}_1} < 103.5$, in violation of the bound from LEP2. The parameter space of the NUHM1

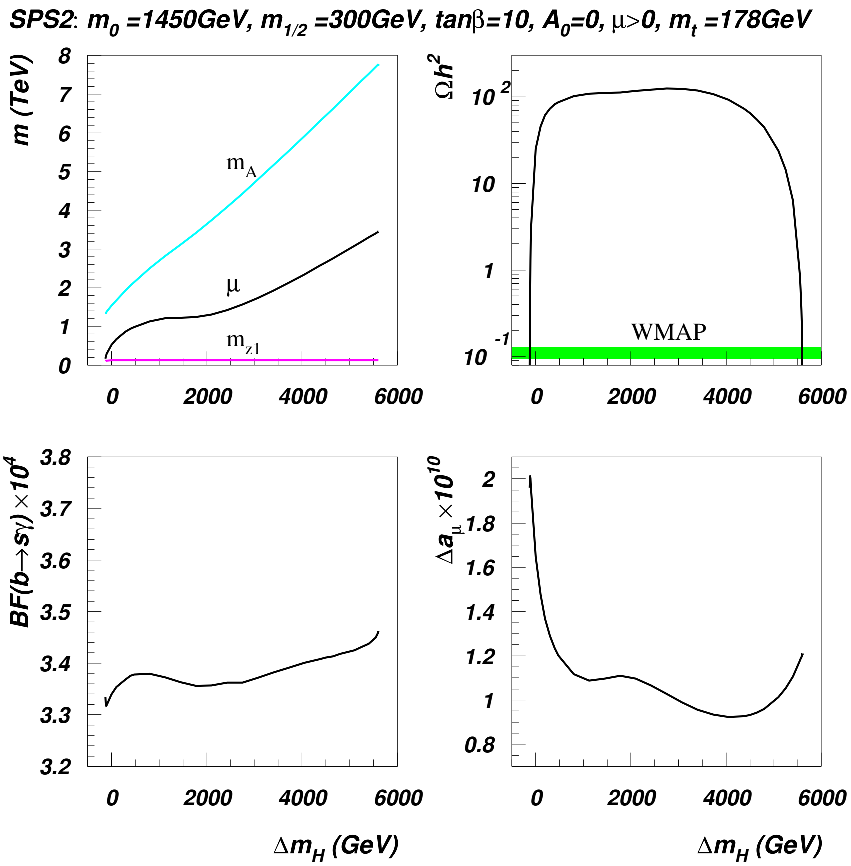

Figure 14: Variation in *a)* m_A, μ and $m_{\widetilde{Z}_1}$, *b)* $\Omega_{\widetilde{Z}_1}h^2$, *c)* $BF(b \to s\gamma)$ and *d)* Δa_μ versus $\Delta m_H \equiv (m_{H_d} - m_{H_u})/2$ in the NUHM2 model, for $m_0 = 1450\,\mathrm{GeV}$, $m_{1/2} = 300\,\mathrm{GeV}$, $A_0 = 0$, $\tan\beta = 10$, $\mu > 0$ and $m_t = 178\,\mathrm{GeV}$.

model is shown by the black dashed line, where $m_{H_u}^2 = m_{H_d}^2$, while the mSUGRA value point where $m_{H_u}^2 = m_{H_d}^2 = m_0^2$ is shown by a black cross. The reader will notice that while the bulk of the parameter space of the NUHM2 model lies *above* this dashed black line where $m_{H_d}^2 > m_{H_u}^2$, there is a small portion for small values of $|m_{H_{u,d}}^2|$ values this is not the case. The reason for this asymmetry is that as seen from the EWSB conditions (2.10) and (2.11), the *weak scale* values of the Higgs mass squared parameters must satisfy $m_{H_d}^2 > m_{H_u}^2$, with $m_{H_u}^2 < 0$: if the former inequality is badly violated at the GUT scale, radiative corrections cannot "correct this", and the correct pattern of EWSB is not obtained. We also show contours of μ (magenta) ranging from 300-2000 GeV, where 300 GeV contour is on the far right-hand side. Contours of m_A ranging from 300-1500 GeV are also shown, increasing from bottom to top. The $\sqrt{\chi^2}$ value is shown in frame *b*), which shows most of the parameter space is excluded. The exception is the narrow green/yellow region near the lower edge of allowed parameter space, which is the A-funnel, and on the right-most edge of parameter space, barely visible, is the higgsino region. The narrow green region at the upper boundary of parameter space corresponds to the slepton (or squark for large m_0) co-annihilation region.

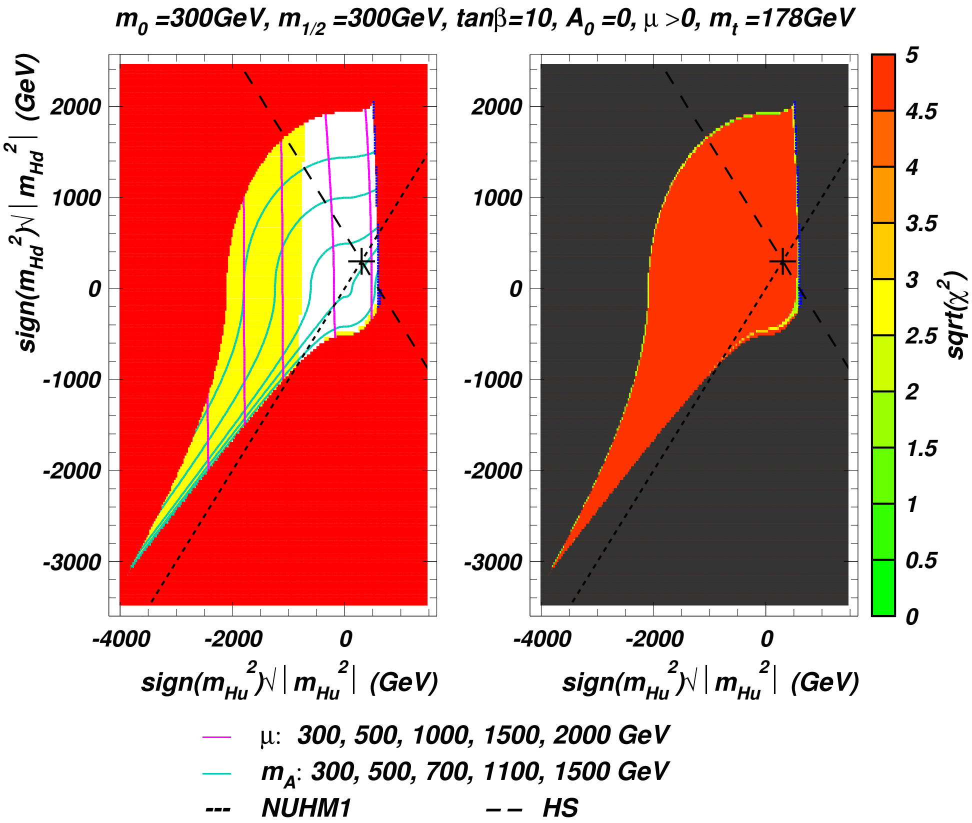

Figure 15: Plot of allowed parameter space in the m_{H_u} vs. m_{H_d} plane of the NUHM2 model for for $m_0 = m_{1/2} = 300\,\text{GeV}$, $A_0 = 0$, $\tan\beta = 10$, $\mu > 0$ and $m_t = 178\,\text{GeV}$. In frame *a*), we show contours of μ and m_A, while in frame *b*) we show values of χ^2. The yellow region in frame *a*) is where so-called "GUT stability bound" is violated. The short-dashed black line denotes the parameter space of the NUHM1 model. The cross denotes the mSUGRA model, while the long-dashed line gives the model where the Higgs scalar mass parameters are split as in figure 11. The blue region is excluded by LEP2.

The DM allowed regions of parameter space show up more prominently if the parameters $m_{H_u}^2$ and $m_{H_d}^2$ are traded for m_A and μ as inputs. We display in figure 16 the $\sqrt{\chi^2}$ values for the same parameter space as in figure 15, but this time in the m_A vs. μ plane. Again most of the parameter space is excluded, although in this mapping the higgsino region shows up as the broad band of green/yellow at low μ values, while the A-annihilation funnel shows up as the vertical band running upwards near $m_A \sim 250\,\text{GeV}$. This plot highlights the importance of the measure of parameter space when deciding the likelihood that any particular framework satisfies some empirical (or, for that matter, theoretical) criteria: the tiny green/yellow sliver along the right edge in figure 15 is expanded into the band, while the thin sliver at the bottom shows up as the A funnel. Notice also the thin green/yellow region for very large m_A values, where the existence of light sleptons brings

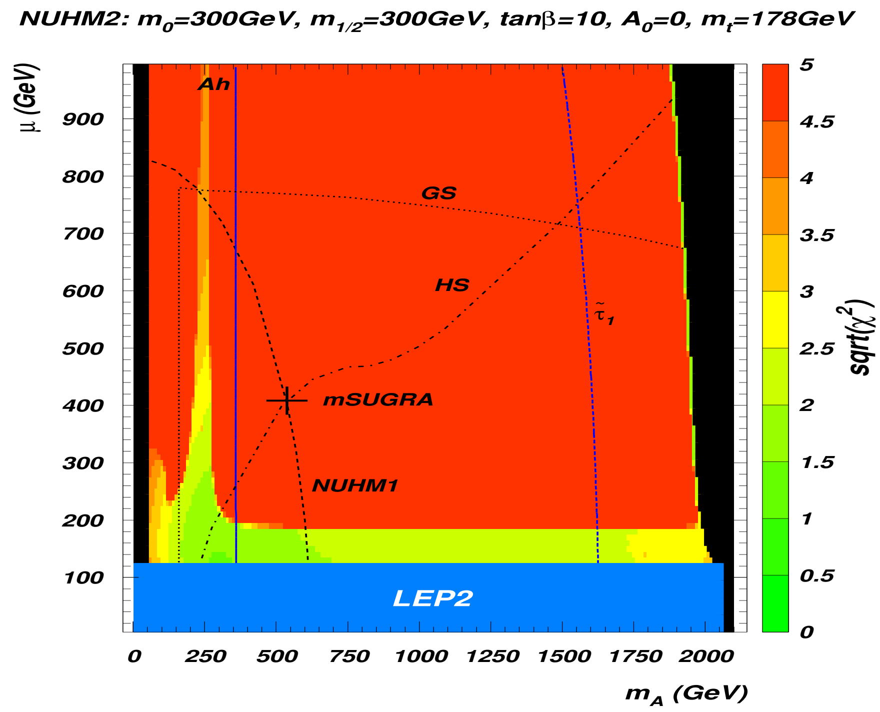

Figure 16: Plot of regions of $\sqrt{\chi^2}$ in the μ vs. m_A plane for $m_0 = m_{1/2} = 300\,\mathrm{GeV}$, $A_0 = 0$, $\tan\beta = 10$ and $m_t = 178\,\mathrm{GeV}$ for $\mu > 0$. The line labeled HS denotes the NUMH2 model where just the Higgs mass parameters are split as in figure 11. The region to the left of the Ah contour is where Ah production is accessible to a $\sqrt{s} = 500\,\mathrm{GeV}$ ILC, while the region to the right of the $\tilde{\tau}_1$ contour is accessible to ILC via stau pair searches.

the relic density prediction into accord with the WMAP value of $\Omega_{CDM}h^2$. The NUHM1 model extends along the black dashed contour arc, with the mSUGRA model denoted by a cross. The regions away from the NUHM1 model arc denote SUSY mass spectra which are phenomenologically different from either the mSUGRA or NUHM1 model. In fact the points with low μ *and* low m_A, which only occur in the NUHM2 model, are somewhat favored by the combined constraints. The regions above and left of the GS contour violate the GS condition, while the HS contour denotes the path of the HS model through the NUHM2 model parameter space.

The predictions for $\Omega_{\tilde{Z}_1}h^2$ and contours for $BF(b \to s\gamma)$ and Δa_μ are separately shown in figure 17 for *a*) $\mu > 0$ and also for the disfavored value *b*) $\mu < 0$. As before, we take $m_0 = m_{1/2} = 300\,\mathrm{GeV}$, $A_0 = 0$, $\tan\beta = 10$ and $m_t = 178\,\mathrm{GeV}$. In frame *a*), the bulk of the allowed parameter space is determined by the WMAP allowed region. Within this region, the values of $BF(b \to s\gamma)$ and Δa_μ determine the best fit, which turns out to be $m_A \sim 300\,\mathrm{GeV}$ and $\mu \sim 130\,\mathrm{GeV}$. In this region, charginos and neutralinos as well as MSSM Higgs bosons are all relatively light. In frame *b*), for $\mu < 0$, it is seen that $BF(b \to s\gamma)$ is $\sim 4 \times 10^{-4}$ in the low right-hand region. For smaller values of $|\mu|$ and m_A, the value of $BF(b \to s\gamma)$ only increases, pushing the χ^2 to large values all over the WMAP allowed region.

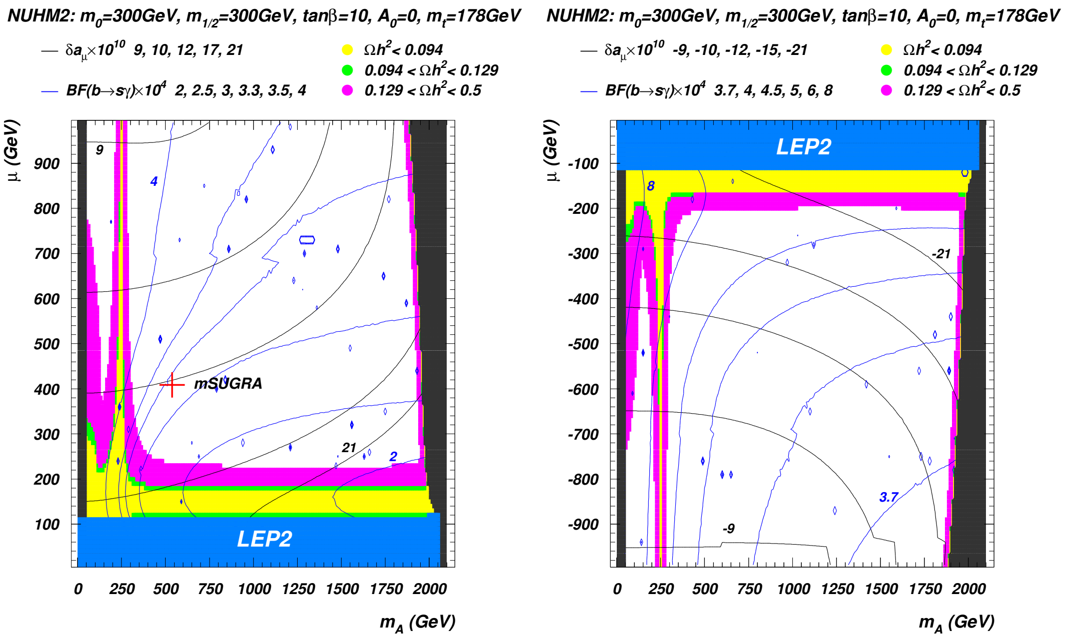

Figure 17: Ranges of $\Omega_{\widetilde{Z}_1} h^2$ together with contours of $BF(b \to s\gamma)$ and Δa_μ in the μ vs. m_A plane for $m_0 = m_{1/2} = 300\,\text{GeV}$, $A_0 = 0$, $\tan\beta = 10$ and $m_t = 178\,\text{GeV}$. For very large values of m_A, we have the stau co-annihilation region. In frame a), we show contours for $\mu < 0$ and in frame b) we show contours for $\mu > 0$.

3.3 Dark matter detection: the NUHM2 model

We show in figure 18 and 19 the reach contours for the various detection channels introduced in section 2.3, respectively for the Burkert Halo Model (figure 18) and for the Adiabatically Contracted N03 Halo Model (figure 19): parameter space points lying below, or to the left, of the reach contours will yield detectable signals via the corresponding searches. The dashed black lines mark the locus of points appropriate to the one-parameter NUHM1 model, where $m_{H_u}^2 = m_{H_d}^2$ at $Q = M_{GUT}$. The red cross indicates the particular point given by the universal mSUGRA case.

For the chosen values of mSUGRA parameters (which include gluino and squark masses up to several hundred GeV), stage-3 direct detection experiments will probe the bulk of the $\mu - m_A$ plane allowed by cosmology, independently of the halo model under consideration. The exception is the region with very large values of $m_A \sim 1.8$ TeV (not shown in the figure) where the relic density is in accord with the WMAP observation because the sleptons become very light. A large portion of the WMAP allowed region will also be within reach of stage-2 detectors, particularly for low values of the μ parameter. The shape of the VR curves is again readily understood in terms of the interplay of the two effects that we discussed in detail in section 2.4: the enhancement of the heavy CP-even Higgs exchange channel at low m_A, and the increased higgsino fraction, at low values of the μ parameter.

The expected flux of muons from neutralino annihilations in the Sun is particularly sensitive to the value of the μ parameter: if the latter is sufficiently low, it provides a large

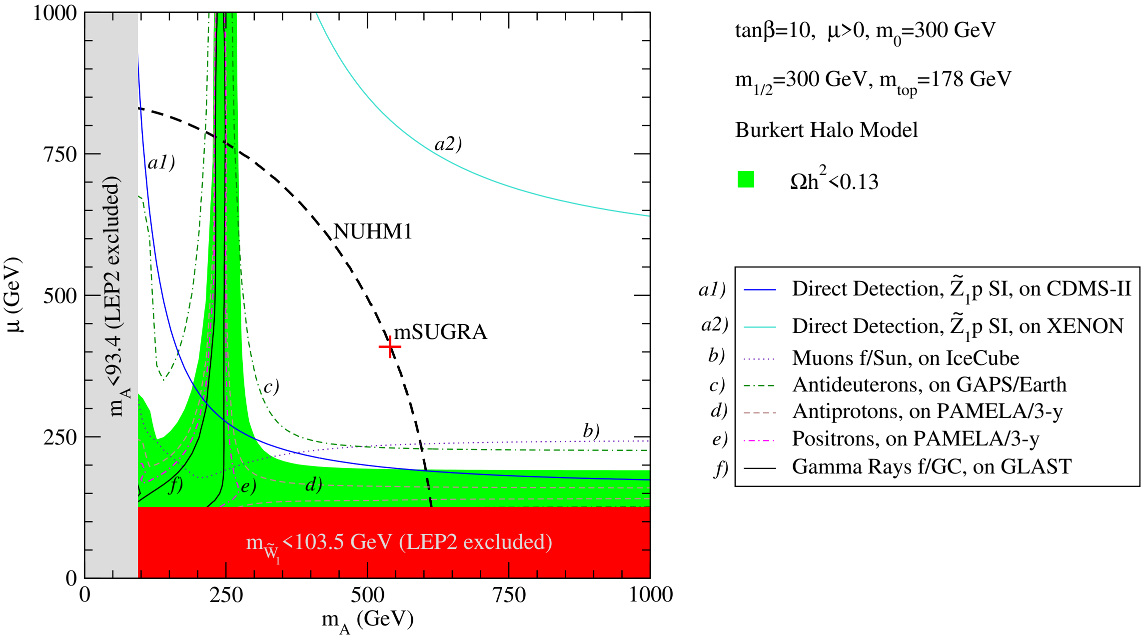

Figure 18: The reach contours (i.e. the iso-VR=1 lines) for various dark matter detection techniques in the (m_A, μ) plane. Points lying to the bottom-left of the lines are within reach of the future experimental facilities, as described in section 2.3. The black dashed line indicates the parameter space of the NUHM1 model in this plane, while the red cross locates the mSUGRA universal case.

enough spin-dependent neutralino-proton scattering cross section and a large capture rate of neutralinos in the core of the Sun, hence giving a large enough signal at IceCube.

A comparison of figures 18 and 19 shows what we had alluded to in the last section: the Burkert halo profile yields conservative predictions for the prospects for detection of relic LSPs. Indirect detection rates essentially track the size of the mass-rescaled pair annihilation rate $\langle\sigma v\rangle/m^2_{\widetilde{Z}_1}$. The difference between the profiles is especially accentuated for gamma rays, where the five orders of magnitude enhancement mentioned in section 2.3 implies that the entire plane will be covered for the Adiabatically Contracted Halo Model. The difference between the models is also considerable for the various antimatter searches, where once again, the Burkert profile leads to the most conservative prediction.

We show in figure 20 ($m_0 = 300\,\mathrm{GeV}$) and figure 21 ($m_0 = 1450\,\mathrm{GeV}$) the neutralino-proton spin-independent scattering cross section $\sigma^{SI}_{\widetilde{Z}_1 p}$ as a function of Δm_H, together with the current experimental limit and the projected sensitivity of Stage-2 and Stage-3 detectors. In both cases, $\sigma^{SI}_{\widetilde{Z}_1 p}$ increases significantly for large negative values of Δm_H, in the region where the neutralino gets a large higgsino fraction since $|\mu|$ becomes small (left panels). Stage-3 direct detection experiments will thoroughly probe the WMAP allowed region in the left part of the plots, and Stage-2 detectors will have access to a wide portion of it. As for the large positive end of the Δm_H range, a WMAP compatible relic abundance is achieved, in both cases, through sfermion co-annihilations. In the $m_0 = 300\,\mathrm{GeV}$ case squarks are heavy, and a light slepton sector does not particularly facilitate direct detection

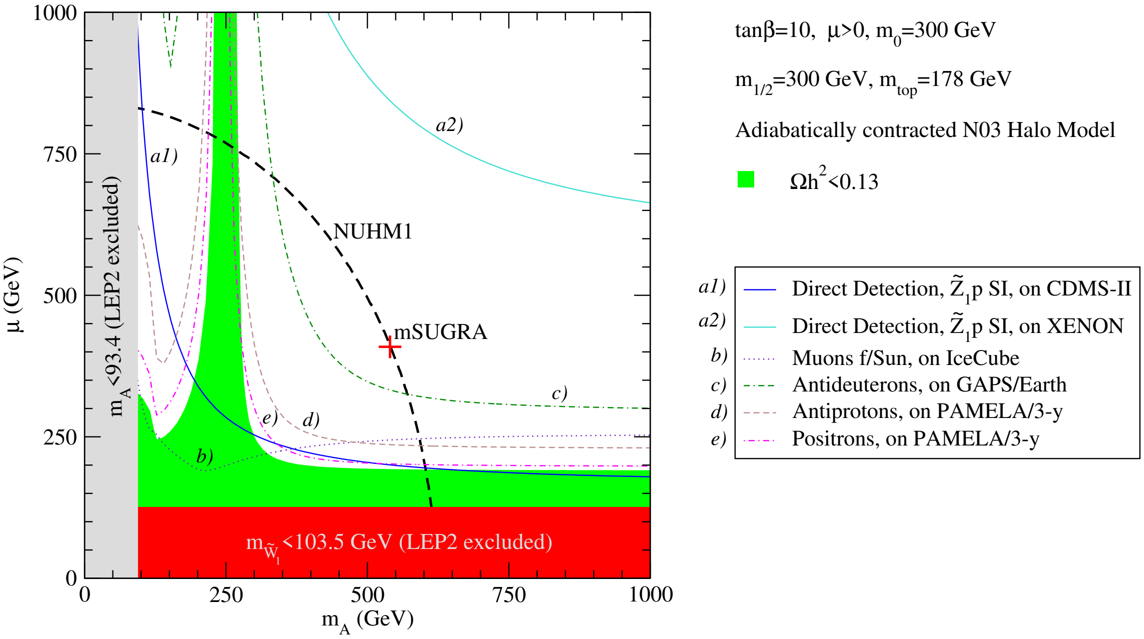

Figure 19: The same as in figure 18, but for the Adiabatically contracted N03 Halo Model. The VR contour for gamma rays from the galactic center is not shown, since the whole parameter space range shown in the figure features a VR larger than 1 in that detection channel (see the discussion in the text).

of the neutralino, which is found to lie even beyond Stage-3 detectors.[8] In the $m_0 = 1450\,\mathrm{GeV}$ case, the co-annihilating partners participate in the neutralino-proton scattering through s-channel squark exchange diagrams. This results in resonant squark contributions to neutralino nucleon scattering which enormously enhance $\sigma^{SI}_{\widetilde{Z}_1 p}$ when $m_{\tilde{q}} \to m_{\widetilde{Z}_1}$. The steepness of $\sigma^{SI}_{\widetilde{Z}_1 p}$ as a function of Δm_H, in the $m_0 = 1450\,\mathrm{GeV}$ case, is further increased by the occurrence of an accidental cancellation between the up-squark neutralino-quark amplitude and the charm-squark gluon-mediated amplitude at $\Delta m_H \simeq 5530$ GeV.

Figure 22 ($m_0 = 300\,\mathrm{GeV}$) and figure 23 ($m_0 = 1450\,\mathrm{GeV}$) show our results for the expected muon flux from the sun for the supersymmetric cases that we have been examining. As for the neutralino-proton spin-independent scattering cross section discussed above, the increase in the higgsino fraction in the left part of the left panels dictates a larger neutralino pair annihilation cross section as well as a larger spin-dependent neutralino-proton scattering cross section. As a result, when the neutralino thermal relic abundance enters the WMAP region, the expected muon flux gets close to or above the IceCube projected sensitivity for a hard neutrino spectrum, and even exceed the Super-Kamiokande limit in the $m_0 = 1450$ GeV case. The abrupt drop in the muon flux visible in the $m_0 = 1450$ GeV figure, close to the LEP-2 chargino mass limit, is due to the gauge bosons

[8]Although we can envision that the neutralino electron scattering may be resonantly enhanced if $m_{\tilde{e}_L} \simeq m_{\widetilde{Z}_1}$, the energy transferred to the electron is very small because the electron is very light. In this respect, the situation is different for the case of scattering off a nucleon discussed below.

JHEP07(2005)065

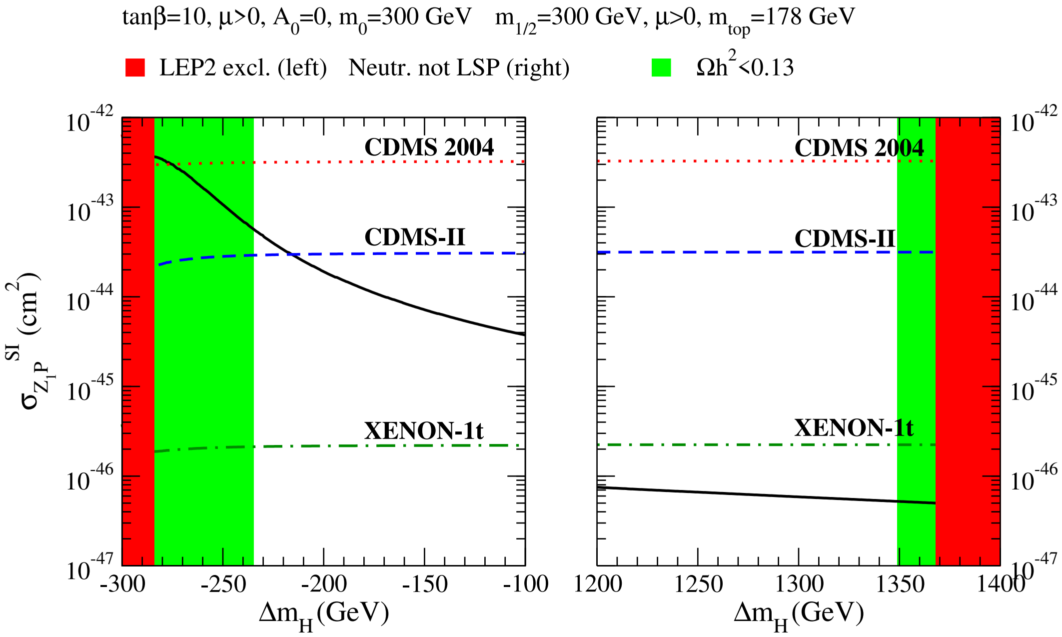

Figure 20: The neutralino-proton spin-independent scattering cross section $\sigma^{SI}_{\widetilde{Z}_1 p}$ as a function of Δm_H (black solid line), at $m_0 = 300\,\mathrm{GeV}$. The other input parameters are specified in the figure. The dotted red line indicates the current 90% CL exclusion limit on $\sigma^{SI}_{\widetilde{Z}_1 p}$ delivered by the CDMS experiment [59], while the blue dashed lines and the green dot-dashed lines correspond to the projected 90%CL exclusion limits for Stage-2 and Stage-3 detectors, taking as benchmark experiments the next-generation CDMS-II detector and the XENON-1 ton facility.

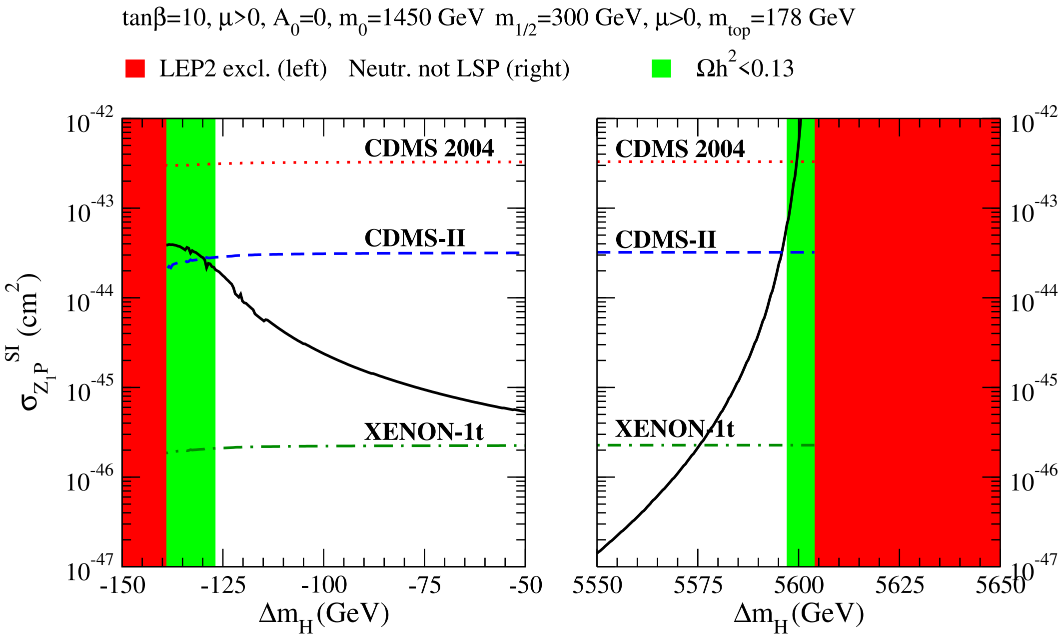

Figure 21: Same as in figure20, but at $m_0 = 1450$ GeV.

JHEP07(2005)065

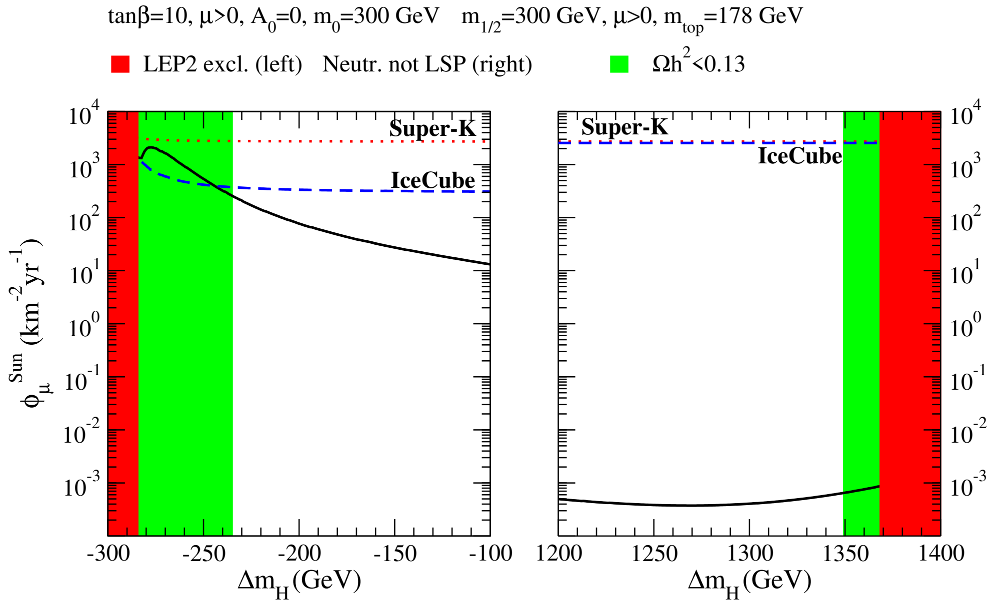

Figure 22: The flux of muons from the Sun generated by charged current interactions of neutrinos produced in the center of the celestial body by neutralino-pair annihilations, integrated above a 1 GeV threshold (solid black line), as a function of Δm_H (black solid line), at $m_0 = 300\,\mathrm{GeV}$, with other parameters as specified in the figure. The red dotted curves indicate the current 90% CL Super-Kamiokande limits on the muon flux from the Sun, while the dashed blue lines the expected 90% CL IceCube sensitivity. We corrected for the energy threshold mismatch in the computation of the projected IceCube exclusion curve, and we used a hard neutrino spectrum in the left panel and a soft neutrino spectrum in the right panel (see the text for details).

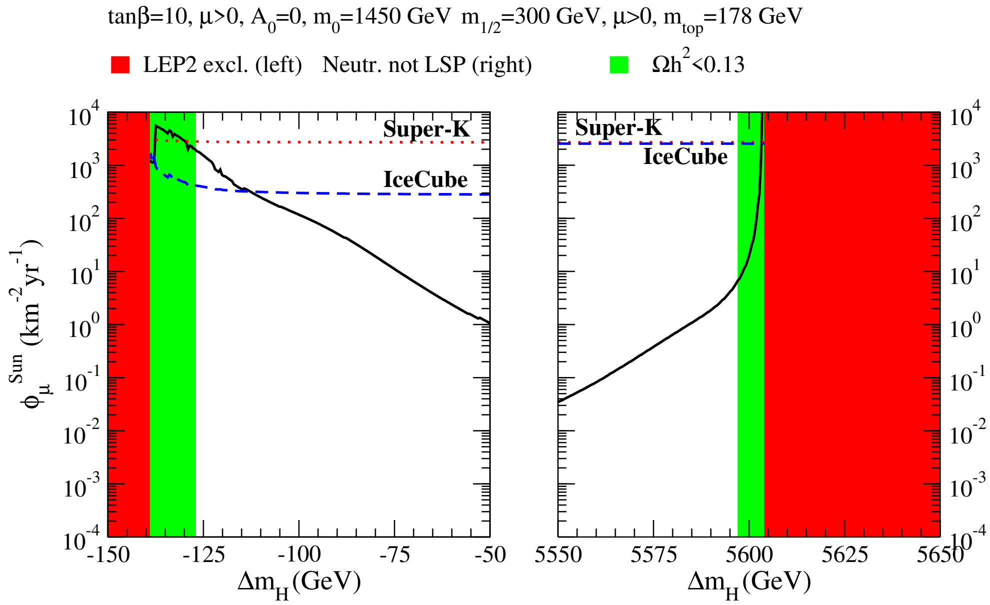

Figure 23: Same as in figure 22, but at $m_0 = 1450$ GeV.

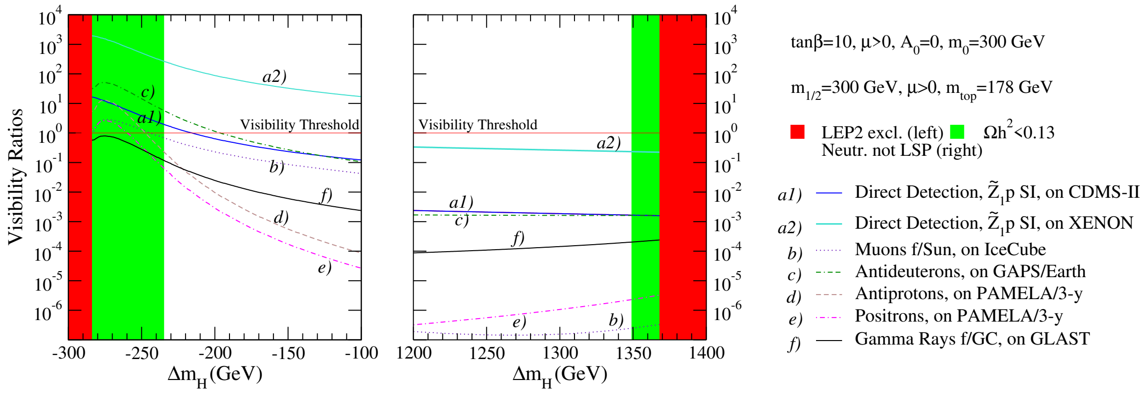

Figure 24: The Dark Matter detection Visibility Ratios (VR) for various detection strategies, as a function of the GUT-scale Higgs mass splitting Δm_H, at $m_0 = 300\,\mathrm{GeV}$. The other input parameters are specified in the figure. When the VR is above the "Visibility Threshold" (i.e. the VR=1 line) the corresponding model is within the reach of the corresponding dark matter search experiment.

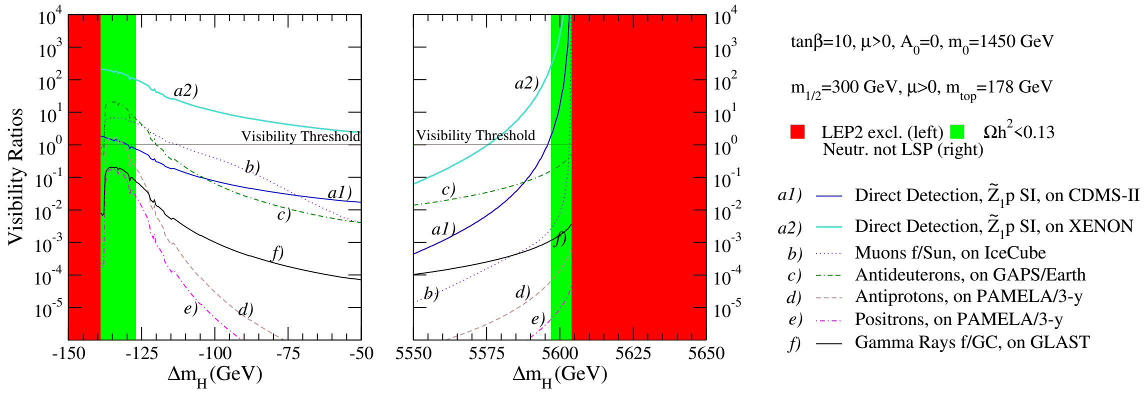

Figure 25: Same as in figure 24, but at $m_0 = 1450$ GeV.

thresholds. As regards the sfermion co-annihilation regions (right panels), light sleptons induce only a slightly larger neutralino pair annihilation cross section (figure 22), while the squark-mediated resonant increase in $\sigma_{\widetilde{Z}_1 p}$ produces an extremely large muon flux in the $m_0 = 1450\,\mathrm{GeV}$ scenario (figure 23).

The overall summary and comparison of direct and indirect dark matter detection methods considered here is shown in figure 24 ($m_0 = 300\,\mathrm{GeV}$) and figure 25 ($m_0 = 1450$ GeV) for the conservative Bukhert profile. This conservative assumption is why, in both cases, the gamma ray flux from the Galactic Center is well below the projected GLAST sensitivity. Antimatter searches will instead produce positive results in the higgsino-like region at negative Δm_H. In particular, antideuteron searches on GAPS look extremely promising in the present setup, as they will entirely probe the WMAP-allowed region for both values of m_0. In the $m_0 = 1450\,\mathrm{GeV}$ scenario (figure 25), as for the muon flux,

JHEP07(2005)065

parameter	NUHM2a	NUHM2b	NUHM2c
m_0	**300**	**300**	**1450**
μ	**220**	933.2	3443.7
m_A	**140**	1884.6	7765.1
$m_{H_d}^2$	$-(506.4)^2$	$\mathbf{(1651.7)^2}$	$\mathbf{(7047.3)^2}$
$m_{H_u}^2$	$-(263.5)^2$	$\mathbf{-(1051.7)^2}$	$\mathbf{-(4147.3)^2}$
$m_{\tilde{g}}$	726.4	739.4	807.8
$m_{\tilde{u}_L}$	720.6	740.4	1724.8
$m_{\tilde{u}_R}$	713.3	591.9	151.6
$m_{\tilde{t}_1}$	491.0	661.9	1802.9
$m_{\tilde{b}_1}$	629.0	730.6	1830.5
$m_{\tilde{e}_L}$	377.6	180.9	660.7
$m_{\tilde{e}_R}$	292.4	546.3	2316.1
$m_{\tilde{\tau}_1}$	290.1	149.3	522.9
$m_{\tilde{\nu}_\tau}$	368.3	129.9	513.1
$m_{\widetilde{W}_2}$	293.8	937.1	3428.8
$m_{\widetilde{W}_1}$	174.4	236.0	250.4
$m_{\widetilde{Z}_4}$	296.4	935.7	3427.1
$m_{\widetilde{Z}_3}$	228.5	931.1	3426.5
$m_{\widetilde{Z}_2}$	178.7	236.1	251.5
$m_{\widetilde{Z}_1}$	108.9	119.2	122.0
m_{H^+}	162.1	1898.6	7816.6
m_h	113.3	116.5	120.3
$\Omega_{\widetilde{Z}_1}h^2$	0.10	0.17	0.14
$BF(b \to s\gamma)$	4.2×10^{-4}	3.3×10^{-4}	3.5×10^{-4}
Δa_μ	15.3×10^{-10}	13.0×10^{-10}	1.2×10^{-10}

Table 2: Masses and parameters in GeV units for three NUHM2 models, where $m_{1/2} = 300\,\mathrm{GeV}$, $A_0 = 0$, $\tan\beta = 10$ and $m_t = 178\,\mathrm{GeV}$. Input parameters are shown as bold-faced.

antimatter fluxes and gamma ray flux undergo a sudden drop motivated by the gauge boson threshold ($m_{\widetilde{Z}_1} < m_W$). Light sfermions help to marginally increase the antimatter rates (see right panels), but the resulting fluxes are found to lie, in all cases, below the expected experimental sensitivity.

3.4 NUHM2 model: Collider searches for SUSY

In this section, we illustrate aspects of the NUHM2 model that lead to collider search possibilities not possible in the NUHM1 model. We illustrate our points by showing in table 2 three cases where the NUHM2 model can be in accord with the WMAP measurement, but which give rise to unique collider phenomenology. All parameter points in this table have the same values of $m_{1/2} = 300\,\mathrm{GeV}$, $A_0 = 0$, $\tan\beta = 10$, $\mu > 0$ and $m_t = 178\,\mathrm{GeV}$. For the first point, labeled NUHM2a, we take $m_0 = 300$ GeV, with $\mu = 220\,\mathrm{GeV}$ and $m_A = 140\,\mathrm{GeV}$. It occurs in the lower-left region of the plot in figure 16 and gives a

JHEP07(2005)065

relic density $\Omega_{\widetilde{Z}_1}h^2 = 0.10$. It is characterized by *both* a low μ and a low m_A value, unlike the NUHM1 model, which must have one or the other small, but not both, to be in accord with WMAP. This point yields light higgsinos *and* light A, H and $H^\pm$ SUSY Higgs bosons. The second point, NUHM2b, has $m_0 = 300\,\mathrm{GeV}$ as well, but has input parameters $m_{H_d}^2 = (1651.7\ \mathrm{GeV})^2$ and $m_{H_u}^2 = -(1051.7\ \mathrm{GeV})^2$. It is characterized by relatively light left-handed sleptons and sneutrinos, due to the large S term in the RGEs. Finally, we show NUHM2c, which has $m_0 = 1450\,\mathrm{GeV}$ with $m_{H_d}^2 = (7047.3\ \mathrm{GeV})^2$ and $m_{H_u}^2 = -(4147.3\ \mathrm{GeV})^2$. It is characterized by the presence of very light $\tilde{u}_R$ and $\tilde{c}_R$ squarks. Notice that the right sleptons are heavier than all the squarks, and that $\tilde{\tau}_1 \simeq \tilde{\tau}_L$ is the lightest of the charged sleptons.[9]

3.4.1 Fermilab Tevatron

The point NUHM2a with low μ and low m_A values will be difficult to probe at the Fermilab Tevatron. In this case, the chargino and neutralino masses are still rather large, and $\widetilde{Z}_2 \to \widetilde{Z}_1 e^+e^-$ has a branching fraction of just 1.5%, so that trilepton signals will be difficult to detect above background. The m_A and $\tan\beta$ values are such that this point lies just beyond a “hole” in parameter space where none of the Higgs bosons are accessible to the Tevatron, even at the 95%CL exclusion level [99, 100]. The point NUHM2b, with relatively light sleptons, will also be difficult to probe at the Tevatron since charginos are quite heavy and slepton pairs are difficult to detect for any mass choices [101]. The point NUHM2c has *two* flavors of relatively light squarks — $\tilde{u}_R$ and $\tilde{c}_R$ — but the squark-neutralino mass gap is rather small. The signal would be identical to the one searched for in ref. [102], except with essentially twice the expected cross section for any given squark and LSP masses since $\sigma(\tilde{c}_R\tilde{c}_R) \simeq \sigma(\tilde{u}_R\tilde{u}_R)$). It is possible that a dedicated squark search might be able to detect a signal in the dijet+ $\not{E}_T$ channel, where relatively low jet E_T and $\not{E}_T$ values $\sim 25 - 50\,\mathrm{GeV}$ might be expected, owing to the small $\tilde{u}_R - \widetilde{Z}_1$ mass gap. Alternatively, if it becomes possible to tag c-jets with significant efficiency, it may be possible to suppress backgrounds sufficiently to pull out the signal. The phenomenology of light $\tilde{u}_R$ and $\tilde{c}_R$ squarks for the Tevatron is discussed more completely in ref. [41].

3.4.2 CERN LHC

Squarks and gluinos would be produced at large rates at the CERN LHC. Their cascade decays would, in general, lead to the production of Higgs bosons in SUSY events. In the NUHM2 model, since the Higgs sector is essentially arbitrary, the heavier Higgs bosons H, A and $H^\pm$ could decay into other sparticles, resulting in characteristic events at the LHC [103]. In the case of the NUHM2a scenario shown in the table, the low value of μ implies the entire spectrum of charginos and neutralinos will be quite light, and accessible via squark and gluino cascade decays. The cascade decays will be much more complex

[9] There might also appear to be a possibility of generating characteristic spectra with S large and positive at the GUT scale, where only $\tilde{\ell}_R$ are light, while gluinos, charginos and neutralinos as well as most squarks and left sleptons would be heavy, making the signal difficult to detect at the LHC. This case does not, however, seem to be possible because large positive S leads to $m_A^2 < 0$ and thus a breakdown in the REWSB mechanism before the $\tilde{e}_R$ becomes light enough.

JHEP07(2005)065

than in a typical mSUGRA scenario, but as for the NUHM1b point discussed earlier, potentially offer a rich possibility for extracting information via a variety of mass edges that would be theoretically present. The feasibility of actually doing so would necessitate detailed simulations beyond the scope of the present analysis. In addition, in this scenario, the heavier Higgs bosons are also quite light, and in fact the heavier inos are able to decay into A, H and $H^\pm$ with significant rates. The production of H and A followed by $H,\ A \to \tau^+\tau^-$ and perhaps also to $\mu^+\mu^-$, should be detectable at the LHC. In addition, Wh or $t\bar{t}h$ production with W and one of the tops decaying leptonically should also be detectable.

The point NUHM2b is characterized by light sleptons. In this case, $\tilde{q}_L$ cascade decays will be lepton-rich, since $\widetilde{Z}_2 \to \tilde{e}_L e$ with a branching ratio $\sim 10\%$, while $\widetilde{W}_1 \to \tilde{\ell}_L\nu + \ell\tilde{\nu}$ essentially 100% of the time. The decay $\widetilde{Z}_2 \to \tilde{\nu}\nu$ is also allowed, but in this case the sneutrino decays invisibly. Gluinos nearly always decay to $\tilde{u}_R u$ or $\tilde{c}_R c$. The squarks then decay via $\tilde{u}_R \to u\widetilde{Z}_1$ and $\tilde{c}_R \to c\widetilde{Z}_1$, so that $\tilde{g}\tilde{g}$ production will give rise to ~ 4 jet + $\not{E}_T$ events.

The point NUHM2c, characterized by light $\tilde{u}_R$ and $\tilde{c}_R$ squarks, will allow for squark production at very large rates. In addition, $\tilde{g}\tilde{g}$ production followed by $\tilde{g} \to \tilde{u}_R u$ or $\tilde{c}_R c$ will give rise to $2-4$-jet + $\not{E}_T$ events, since the jets from $\tilde{u}_R \to u\widetilde{Z}_1$ decay will be rather soft owing to the small $\tilde{u}_R - \widetilde{Z}_1$ mass gap. The cascade decay events in this case will be lepton-poor since $\widetilde{Z}_2$ decays mostly to $\widetilde{Z}_1 h$ or $\tilde{u}_R u,\ \tilde{c}_R c$ final states, and $\tilde{q}_L$ is heavy so that charginos are not abundantly produced via their decays.

3.4.3 Linear e^+e^- collider

Any scenario similar to that represented by point NUHM2a would be a bonanza for the ILC. In this case, a $\sqrt{s} = 0.5-0.6\,\text{TeV}$ machine would be able to access both chargino and all four neutralino states as well as the heavy Higgs bosons H, A and $H^\pm$. The difficulty would be in sorting out the large number of competing reactions, but here, variable center of mass energy and beam polarization would be a huge help. A complete reconstruction of chargino and neutralino mass matrices may be possible [104]. The low value of m_A should serve to distinguish this case from a NUHM1a-like scenario.

In the case of NUHM2b, the $\tilde{\tau}_1$ and $\tilde{e}_L$ slepton states would be accessible to early searches, along with $\widetilde{W}_1^+\widetilde{W}_1^-$ production. Beam polarization would be a key ingredient in determining that the $\tilde{\tau}_1$ and $\tilde{e}_L$ are left-handed. Determination that $\tilde{\tau}_1$ is dominantly $\tilde{\tau}_L$ and/or $m_{\tilde{e}_L} \ll m_{\tilde{e}_R}$ would already point to an unconventional scenario.

The case of NUHM2c would allow $\tilde{u}_R\bar{\tilde{u}}_R$ and $\tilde{c}_R\bar{\tilde{c}}_R$ production to occur at large rates at an ILC. Again, the beam polarization would easily determine the right-hand nature of these squarks, which would be a key measurement. It should also be possible to determine their masses [105], and if it is possible to tag c jets with reasonable efficiency, to also distinguish between squark flavors.

We note here that in addition, in the NUHM2 model, the reach of an ILC may be far greater than the CERN LHC for supersymmetry. The reason is that the LHC reach is mainly determined by the m_0 and $m_{1/2}$ parameters, which determine the overall squark and gluino mass scales. In contrast, the ILC reach for chargino pair production depends

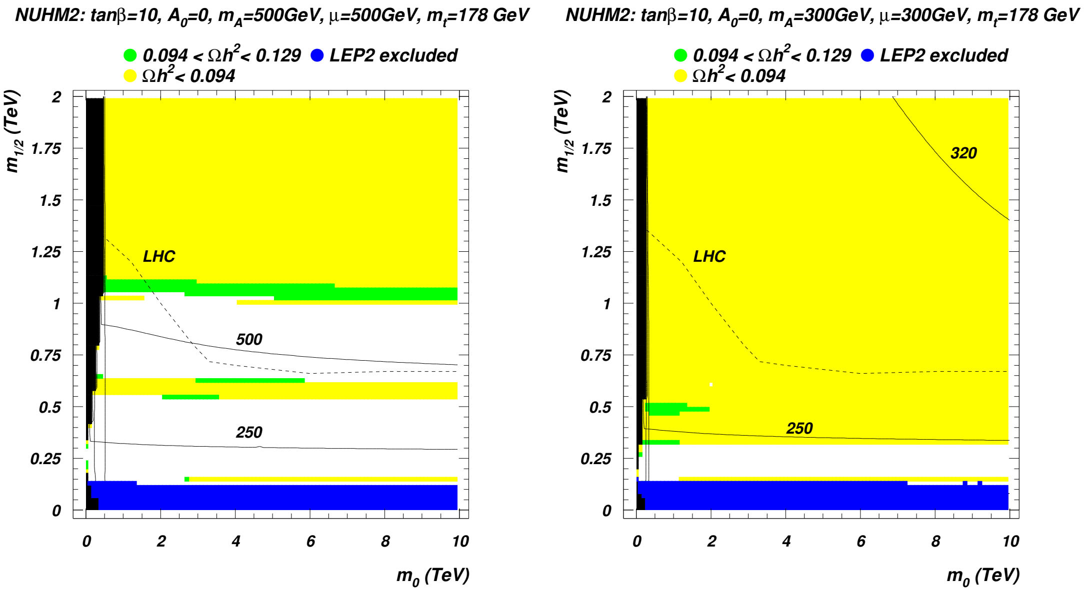

Figure 26: Approximate reach of the CERN LHC (100 fb^{-1}) and ILC for supersymmetric matter in the NUHM2 model in the m_0 vs. $m_{1/2}$ plane for $\tan\beta = 10$, $A_0 = 0$, $\mu > 0$ and $m_t = 178\,\mathrm{GeV}$, for *a*) $\mu = 500\,\mathrm{GeV}$, $m_A = 500\,\mathrm{GeV}$ and *b*) $\mu = 300\,\mathrm{GeV}$, $m_A = 300\,\mathrm{GeV}$.

strongly on the μ parameter. Thus, the NUHM2 case where m_0 and $m_{1/2}$ are large, while μ is small may mean chargino pair production is accessible to an ILC while gluino and squark pair production is beyond LHC reach. The case is illustrated in figure 26, where we show the m_0 vs. $m_{1/2}$ plane for $A_0 = 0$, $\tan\beta = 10$, $\mu > 0$ $m_t = 178\,\mathrm{GeV}$ and *a*) $\mu = m_A = 500\,\mathrm{GeV}$ and *b*) $\mu = m_A = 300\,\mathrm{GeV}$. The yellow and green regions are WMAP allowed, while the unshaded regions have $\Omega_{\widetilde{Z}_1}h^2$ bigger than the WMAP upper bound. The yellow bands just above the LEP excluded blue regions in both frames is where $2m_{\widetilde{Z}_1} \simeq m_h$. The corresponding band in the left panel at $m_{1/2} \simeq 0.6$ TeV is the A funnel, while in the upper yellow/green regions in both panels the LSP has a significant higgsino content.

The SUSY reach of the CERN LHC should be similar to the case of the mSUGRA model calculated in ref. [91], and as before, we show this result as an approximate depiction of the LHC reach for the case for the NUHM2 model. We also show the mass contour in *a*) for a 250 and 500 GeV chargino, accessible to a $\sqrt{s} = 0.5$ or 1 TeV ILC machine. Here, the 1 TeV machine has a reach beyond the large m_0 reach of the LHC. In the case of frame *b*), μ is so small that the $\widetilde{W}_1$ mass is almost always below $\sim 330\,\mathrm{GeV}$, and so the entire plane shown would be accessible to a 1 TeV ILC!

4. Concluding Remarks

We have examined the phenomenological implications of gravity-mediated SUSY breaking models with universal matter scalars, but with non-universal Higgs soft SUSY breaking masses. For simplicity, we assume a common GUT scale mass parameter for *all* matter scalars — this guarantees that phenomenological constraints from flavor physics are respected — but unlike in mSUGRA, entertain the possibility that the soft SUSY breaking mass parameters in the Higgs sector are unrelated to the matter scalar mass. In these non-universal Higgs mass (NUHM) models where the Higgs fields H_u and H_d originate in a common multiplet (as, for instance, in an SO(10) model with a single Higgs field), we would have $m_{H_u}^2 = m_{H_d}^2$, and there would be just one additional new parameter (NUHM1 model) [25] *vis à vis* mSUGRA, while the more general scenario would have two additional parameters (NUHM2 model). We have found that, once WMAP constraints are incorporated into the analysis, this seemingly innocuous extension of the mSUGRA parameter space, which naively would not be expected to affect squark, gluino and slepton masses, significantly expands the possibilities for LHC and linear collider phenomenology from mSUGRA expectations: phenomena that were considered unlikely because they were expected to occur only in particular corners of parameter space become mainstream in the extended model. In the absence of any compelling theory of sparticle masses, the necessity for ensuring that all experimental possibilities are covered is sufficient reason to examine the consequences of NUHM models, regardless of whether or not one considers these to be theoretically attractive.

We have examined the allowed parameter space of the NUHM models with respect to neutralino relic density (WMAP), $BF(b \to s\gamma)$ and Δa_μ constraints. The WMAP upper bound on $\Omega_{CDM}h^2$ requires rather efficient LSP annihilation, and so severely restricts any supersymmetric model. Aside from the bulk region with small values of bino and scalar masses, enhanced LSP annihilation may occur if the LSP has significant higgsino or wino components (the latter is not possible in models with unified gaugino masses[10]), resonantly annihilates via Higgs scalars (or Z bosons), or co-annihilates with the stau or some other charged sparticle. Within mSUGRA, the higgsino annihilation region occurs only if m_0 is very large, while resonance annihilation with heavy Higgs scalars is possible only for large values of $\tan\beta$. However, even in the simple one parameter NUHM1 extension of mSUGRA, for almost any values of m_0, $m_{1/2}$ and $\tan\beta$, there are two different choices of m_ϕ (defined in the text) that can bring the relic density to be in accord with the WMAP measurement: for large positive m_ϕ, one enters the higgsino region, while for large negative values of m_ϕ, one enters the A annihilation funnel. The higgsino region with small μ values gives rise to large rates for direct and indirect detection of neutralino dark matter, and also leads to light charginos and neutralinos which might be accessible to a TeV-scale linear e^+e^- collider, or which can enrich the gluino and squark cascade decays expected at the CERN LHC. The A-funnel region in the NUHM1 model can also occur at any $\tan\beta$ value, and usually leads to relatively light H, A and $H^\pm$ Higgs bosons which may be accessible to collider searches. Also, the expected suppression of e and μ signals from cascade decays, which is expected in the mSUGRA model for points in the A-funnel due to enhanced -ino decays to taus [107], will not necessarily obtain in the NUHM1 model since $\tan\beta$ is not required to be large. Since the early universe neutralino pair annihilation cross sections are enhanced on the A-resonance, indirect DM signals are, in general, enhanced as well.

[10]For an exception to this, see the **200** model in ref.[106].

The parameter freedom is enhanced even more in the NUHM2 model. In this case, the mSUGRA-fixed parameters μ and m_A can now be taken as inputs, rather than outputs. This allows one to always dial in a low value of μ such that one is in the higgsino region, or a low value of m_A so that one is in the A-funnel. As before, direct and indirect DM detection rates are enhanced in these regions. Collider signals may change as well, since now *all* charginos and neutralinos can be light, and one can have enhanced cascade decays of squarks and gluinos to charginos, neutralinos *and* to heavy Higgs bosons. In the case where m_0 and $m_{1/2}$ are large, but μ is small, the reach of a LC may exceed that of the CERN LHC. In the NUHM2 model, qualitatively new regions emerge where the relic density is suppressed due to novel sparticle mass patterns: very light left-handed sleptons, or very light right-handed up and charm squarks, which have obvious implications for collider signals. The latter case results in large rates for direct and indirect detection of neutralino DM, in addition to large $jet+\not{E}_T$ signals at hadron colliders, and to the possibility of squark NLSPs at e^+e^- LCs.

In conclusion, we have demonstrated that the seemingly innocuous decoupling of scalar Higgs mass parameters from other scalar masses can significantly alter our expectations of what we may expect in terms of dark matter as well as (s)particle physics phenomenology. This is partly because altering the Higgs potential can dramatically change the value of μ^2 that yields the correct value of M_Z^2, and partly because renormalization group evolution of sparticle mass parameters is dramatically altered by a non-zero value of S in the NUHM2 model. We have found that, for both the NUHM1 and NUHM2 extensions of the mSUGRA model, one is able to find generic regions of parameter space that are in good agreement with the WMAP determination of the cold dark matter relic density, as well as with constraints from $b \to s\gamma$ and $(g-2)_\mu$. These regions, as we show, can lead to distinctive signals at both direct and indirect dark matter detection experiments, and also provide distinctive signatures at both the CERN LHC pp collider and the International Linear Collider, with a center of mass energy $\sqrt{s} = 0.5 - 1\,\text{TeV}$. .

Acknowledgments

This research was supported in part by grants from the U.S. Department of Energy.

References

[1] A.H. Chamseddine, R. Arnowitt and P. Nath, *Locally supersymmetric grand unification*, *Phys. Rev. Lett.* **49** (1982) 970;
R. Barbieri, S. Ferrara and C.A. Savoy, *Gauge models with spontaneously broken local supersymmetry*, *Phys. Lett.* **B 119** (1982) 343;
N. Ohta, *Grand unified theories based on local supersymmetry*, *Prog. Theor. Phys.* **70** (1983) 542;
L.J. Hall, J. Lykken and S. Weinberg, *Supergravity as the messenger of supersymmetry breaking*, *Phys. Rev.* **D 27** (1983) 2359;
for reviews, see H.P. Nilles, *Supersymmetry, supergravity and particle physics*, *Phys. Rept.* **110** (1984) 1 and P. Nath, *Twenty years of sugra*, `hep-ph/0307123`.

[2] For a text book review of supersymmetry see M. Drees, R. Godbole and P. Roy, *Theory and phenomenology of sparticles*, World Scientific, 2005;
for reviews of SUSY phenomenology, see, S.P. Martin, *A supersymmetry primer*, hep-ph/9709356;
M. Drees, *An introduction to supersymmetry*, hep-ph/9611409;
X. Tata, *What is supersymmetry and how do we find it?*, hep-ph/9706307;
S. Dawson, *The MSSM and why it works*, hep-ph/9712464.

[3] S. Dimopoulos and H. Georgi, *Softly broken supersymmetry and* SU(5), *Nucl. Phys.* **B 193** (1981) 150.

[4] S.K. Soni and H.A. Weldon, *Analysis of the supersymmetry breaking induced by $N = 1$ supergravity theories*, *Phys. Lett.* **B 126** (1983) 215;
V.S. Kaplunovsky and J. Louis, *Model independent analysis of soft terms in effective supergravity and in string theory*, *Phys. Lett.* **B 306** (1993) 269 [hep-th/9303040];
K. Choi, J.S. Lee and C. Muñoz, *Supergravity radiative effects on soft terms and the mu term*, *Phys. Rev. Lett.* **80** (1998) 3686 [hep-ph/9709250].

[5] See e.g. J.A. Bagger, *Weak-scale supersymmetry: theory and practice*, hep-ph/9604232.

[6] See constraints in e.g. H. Baer, A. Belyaev, T. Krupovnickas and A. Mustafayev, *SUSY normal scalar mass hierarchy reconciles $(g-2)_\mu, b \to s\gamma$ and relic density*, *JHEP* **06** (2004) 044 [hep-ph/0403214];
see also M. Misiak, S. Pokorski and J. Rosiek, *Supersymmetry and fcnc effects*, *Adv. Ser. Direct. High Energy Phys.* **15** (1998) 795–828 [hep-ph/9703442].

[7] H. Baer, C. Balazs, A. Belyaev, J. Mizukoshi, X. Tata and Y. Wang, *JHEP* **0207** (2002) 050 [hep-ph/0205325];
H. Baer et al., *Updated constraints on the minimal supergravity model. V*, hep-ph/0210441;
for a review, see G. Eigen, R. Gaitskell, G.D. Kribs and K.T. Matchev, *Indirect investigations of supersymmetry*, *eConf* **C010630** (2001) P342 [hep-ph/0112312].

[8] Belle collaboration, K. Abe et al., *A measurement of the branching fraction for the inclusive $b \to x/s$ gamma decays with belle*, *Phys. Lett.* **B 511** (2001) 151 [hep-ex/0103042];
CLEO collaboration, D. Cronin-Hennessy et al., *Hadronic mass moments in inclusive semileptonic b meson decays*, *Phys. Rev. Lett.* **87** (2001) 251808 [hep-ex/0108033];
ALEPH collaboration, R. Barate et al., *A measurement of the inclusive $b \to s\gamma$ branching ratio*, *Phys. Lett.* **B 429** (1998) 169.

[9] Muon g-2 collaboration, G.W. Bennett et al., *Measurement of the positive muon anomalous magnetic moment to 0.7-ppm*, *Phys. Rev. Lett.* **89** (2002) 101804 [hep-ex/0208001].

[10] M. Davier, S. Eidelman, A. Hocker and Z. Zhang, *Updated estimate of the muon magnetic moment using revised results from e^+e^- annihilation*, *Eur. Phys. J.* **C 31** (2003) 503 [hep-ph/0308213];
K. Hagiwara, A.D. Martin, D. Nomura and T. Teubner, *Predictions for g-2 of the muon and alpha(qed)(m(z**2))*, *Phys. Rev.* **D 69** (2004) 093003 [hep-ph/0312250].

[11] D.N. Spergel et al., *Determination of Cosmological Parameters*, *Astrophys. J.* **148** (2003) 175.

[12] J.R. Ellis, K.A. Olive, Y. Santoso and V.C. Spanos, *Supersymmetric dark matter in light of wmap*, *Phys. Lett.* **B 565** (2003) 176 [hep-ph/0303043].

[13] H. Baer, C. Balazs and A. Belyaev, *Neutralino relic density in minimal supergravity with co-annihilations*, *JHEP* **03** (2002) 042 [hep-ph/0202076].

[14] H. Baer and C. Balazs, *Chi $**2$ analysis of the minimal supergravity model including WMAP, $g_m u - 2 and b \to s\gamma$ constraints*, *JCAP* **05** (2003) 006 [hep-ph/0303114].

[15] A.B. Lahanas and D.V. Nanopoulos, *WMAPing out supersymmetric dark matter and phenomenology*, *Phys. Lett.* **B 568** (2003) 55 [hep-ph/0303130];
for a review, see A.B. Lahanas, N.E. Mavromatos and D.V. Nanopoulos, *WMAPing the Universe: supersymmetry, dark matter, dark energy, proton decay and collider physics*, *Int. J. Mod. Phys.* **D 12** (2003) 1529 [hep-ph/0308251].

[16] J.R. Ellis, T. Falk and K.A. Olive, *Neutralino stau coannihilation and the cosmological upper limit on the mass of the lightest supersymmetric particle*, *Phys. Lett.* **B 444** (1998) 367 [hep-ph/9810360];
J.R Ellis, T. Falk, K. Olive and M. Srednicki, *Calculations of neutralino-stau coannihilation channels and the cosmologically relevant region of MSSM parameter space*, *Astropart. Phys.* **13** (2000) 181 [hep-ph/9905481];
M.E. Gomez, G. Lazarides and C. Pallis, *Yukawa unification, $b \to s\gamma$ and bino stau coannihilation*, *Phys. Lett.* **B 487** (2000) 313 [hep-ph/0004028];
R. Arnowitt, B. Dutta and Y. Santoso, *Coannihilation effects in supergravity and D-brane models*, *Nucl. Phys.* **B 606** (2001) 59 [hep-ph/0102181];
H. Baer, C. Balazs and A. Belyaev, ref. [13].

[17] C. Boehm, A. Djouadi and M. Drees, *Light scalar top quarks and supersymmetric dark matter*, *Phys. Rev.* **D 62** (2000) 035012 [hep-ph/9911496];
J. Ellis, K. Olive and Y. Santoso, *Calculations of neutralino-stop coannihilation in the CMSSM*, *Astropart. Phys.* **18** (2003) 395 [hep-ph/0112113];
J. Edsjö, et al., *Accurate relic densities with neutralino, chargino and sfermion coannihilations in mSUGRA*, *JCAP* **04** (2003) 001 [hep-ph/0301106].

[18] K.L. Chan, U. Chattopadhyay and P. Nath, *Naturalness, weak scale supersymmetry and the prospect for the observation of supersymmetry at the Tevatron and at the LHC*, *Phys. Rev.* **D 58** (1998) 096004 [hep-ph/9710473].

[19] J.L. Feng, K.T. Matchev and T. Moroi, *Multi-TeV scalars are natural in minimal supergravity*, *Phys. Rev. Lett.* **84** (2000) 2322 [hep-ph/9908309];
J.L. Feng, K.T. Matchev and F. Wilczek, *Neutralino dark matter in focus point supersymmetry*, *Phys. Lett.* **B 482** (2000) 388 [hep-ph/0004043].

[20] The HB/FP region also appears in H. Baer, C.-h. Chen, C. Kao and X. Tata, *Supersymmetry reach of an upgraded Tevatron collider*, *Phys. Rev.* **D 52** (1995) 1565 [hep-ph/9504234].

[21] M. Drees and M.M. Nojiri, *The neutralino relic density in minimal $N = 1$ supergravity*, *Phys. Rev.* **D 47** (1993) 376 [hep-ph/9207234];
H. Baer and M. Brhlik, *Neutralino dark matter in minimal supergravity: direct detection vs. collider searches*, *Phys. Rev.* **D 57** (1998) 567 [hep-ph/9706509];
P. Quintana and X. Tata, *Yukawa unified supersymmetric* SO(10) *model: cosmology, rare decays and collider searches*, *Phys. Rev.* **D 63** (2001) 015007 [hep-ph/0005027];
H. Baer et al., *Yukawa unified supersymmetric* SO(10) *model: cosmology, rare decays and collider searches*, *Phys. Rev.* **D 63** (2001) 015007 [hep-ph/0005027];

A. Djouadi, M. Drees and J.L. Kneur, *Constraints on the minimal supergravity model and prospects for SUSY particle production at future linear e^+e^- colliders*, *JHEP* **08** (2001) 055 [hep-ph/0107316];
J.R. Ellis, T. Falk, G. Ganis, K.A. Olive and M. Srednicki, *The CMSSM parameter space at large* $\tan\beta$, *Phys. Lett.* **B 510** (2001) 236 [hep-ph/0102098];
L. Roszkowski, R. Ruiz de Austri and T. Nihei, *New cosmological and experimental constraints on the CMSSM*, *JHEP* **08** (2001) 024 [hep-ph/0106334];
A.B. Lahanas and V.C. Spanos, *Implications of the pseudo-scalar Higgs boson in determining the neutralino dark matter*, *Eur. Phys. J.* **C 23** (2002) 185 [hep-ph/0106345].

[22] R. Arnowitt and P. Nath, *Cosmological constraints and* SU(5) *supergravity grand unification*, *Phys. Lett.* **B 299** (1993) 58 [hep-ph/9302317];
H. Baer and M. Brhlik, *Cosmological relic density from minimal supergravity with implications for collider physics*, *Phys. Rev.* **D 53** (1996) 597 [hep-ph/9508321].

[23] F.E. Paige, S.D. Protopescu, H. Baer and X. Tata, *Isajet 7.69: a monte carlo event generator for p p, $\bar{p}p$ and e^+e^- reactions*, hep-ph/0312045.

[24] P. Gondolo et al., *Darksusy: computing supersymmetric dark matter properties numerically*, *JCAP* **07** (2004) 008 [astro-ph/0406204].

[25] H. Baer, A. Mustafayev, S. Profumo, A. Belyaev and X. Tata, *Neutralino cold dark matter in a one parameter extension of the minimal supergravity model*, *Phys. Rev.* **D 71** (2005) 095008 [hep-ph/0412059].

[26] H. Baer and J. O'Farrill, *Probing neutralino resonance annihilation via indirect detection of dark matter*, *JCAP* **04** (2004) 005 [hep-ph/0312350];
H. Baer, A. Belyaev, T. Krupovnickas and J. O'Farrill, *Indirect, direct and collider detection of neutralino dark matter*, *JCAP* **08** (2004) 005 [hep-ph/0405210].

[27] V. Berezinsky, A. Bottino, J. Ellis, N. Fornengo, G. Mignola and S. Scopel, *Neutralino dark matter in supersymmetric models with non-universal scalar mass terms*, *Astropart. Phys.* **5** (1996) 1 [hep-ph/9508249].

[28] V. Berezinsky, A. Bottino, J. Ellis, N. Fornengo, G. Mignola and S. Scopel, *Searching for relic neutralinos using neutrino telescopes*, *Astropart. Phys.* **5** (1996) 333 [hep-ph/9603342]; for a summary, see N. Fornengo, *Neutralino dark matter in non-universal SUSY models*, *Nucl. Phys.* **52A** *(Proc. Suppl.)* (1997) 239.

[29] P. Nath and R. Arnowitt, *Non-universal soft SUSY breaking and dark matter*, *Phys. Rev.* **D 56** (1997) 2820 [hep-ph/9701301].

[30] A. Bottino, F. Donato, N. Fornengo and S. Scopel, *Compatibility of the new dama/nai data on an annual modulation effect in wimp direct search with a relic neutralino in supergravity schemes*, *Phys. Rev.* **D 59** (1999) 095004 [hep-ph/9808459].

[31] A. Bottino, F. Donato, N. Fornengo and S. Scopel, *Probing the supersymmetric parameter space by WIMP direct detection*, *Phys. Rev.* **D 63** (2001) 125003 [hep-ph/0010203].

[32] J.R. Ellis, K.A. Olive and Y. Santoso, *The MSSM parameter space with non-universal Higgs masses*, *Phys. Lett.* **B 539** (2002) 107 [hep-ph/0204192];
J.R. Ellis, T. Falk, K.A. Olive and Y. Santoso, *Exploration of the MSSM with non-universal Higgs masses*, *Nucl. Phys.* **B 652** (2003) 259 [hep-ph/0210205].

[33] J.R. Ellis, A. Ferstl, K.A. Olive and Y. Santoso, *Direct detection of dark matter in the MSSM with non- universal Higgs masses*, *Phys. Rev.* **D 67** (2003) 123502 [hep-ph/0302032].

JHEP07(2005)065

[34] V.D. Barger, F. Halzen, D. Hooper and C. Kao, *Indirect search for neutralino dark matter with high energy neutrinos*, *Phys. Rev.* **D 65** (2002) 075022 [hep-ph/0105182].

[35] D.G. Cerdeno, E. Gabrielli, M.E. Gomez and C. Muñoz, *Neutralino nucleon cross section and charge and colour breaking constraints*, *JHEP* **06** (2003) 030 [hep-ph/0304115];
D.G. Cerdeno and C. Muñoz, *Neutralino dark matter in supergravity theories with non-universal scalar and gaugino masses*, *JHEP* **10** (2004) 015 [hep-ph/0405057].

[36] Y. Mambrini and C. Muñoz, *Gamma-ray detection from neutralino annihilation in non-universal sugra scenarios*, hep-ph/0407158.

[37] J. Ferrandis, *Mass predictions based on a supersymmetric* SU(5) *fixed point*, *Phys. Rev.* **D 68** (2003) 015001 [hep-ph/0211370].

[38] T. Falk, K.A. Olive, L. Roszkowski, A. Singh and M. Srednicki, *Constraints from inflation and reheating on superpartner masses*, *Phys. Lett.* **B 396** (1997) 50 [hep-ph/9611325].

[39] M. Drees, *Supersymmetric dark matter 2004*, hep-ph/0410113.

[40] J.R. Ellis, K.A. Olive, Y. Santoso and V.C. Spanos, *Likelihood analysis of the CMSSM parameter space*, *Phys. Rev.* **D 69** (2004) 095004 [hep-ph/0310356].

[41] D. Auto, H. Baer, A. Belyaev and T. Krupovnickas, *Reconciling neutralino relic density with yukawa unified supersymmetric models*, *JHEP* **10** (2004) 066 [hep-ph/0407165].

[42] H. Baer and M. Brhlik, *QCD improved $b \to s\gamma$ constraints on the minimal supergravity model*, *Phys. Rev.* **D 55** (1997) 3201 [hep-ph/9610224];
H. Baer, M. Brhlik, D. Castano and X. Tata, *$b \to s\gamma$ constraints on the minimal supergravity model with large* $\tan\beta$, *Phys. Rev.* **D 58** (1998) 015007 [hep-ph/9712305].

[43] H. Baer, C. Balazs, J. Ferrandis and X. Tata, *Impact of muon anomalous magnetic moment on supersymmetric models*, *Phys. Rev.* **D 64** (2001) 035004 [hep-ph/0103280].

[44] S. Profumo and P. Ullio, *The role of antimatter searches in the hunt for supersymmetric dark matter*, *JCAP* **07** (2004) 006 [hep-ph/0406018].

[45] S. Profumo and C.E. Yaguna, *A statistical analysis of supersymmetric dark matter in the MSSM after wmap*, *Phys. Rev.* **D 70** (2004) 095004 [hep-ph/0407036].

[46] A. Masiero, S. Profumo and P. Ullio, *Neutralino dark matter detection in split supersymmetry scenarios*, *Nucl. Phys.* **B 712** (2005) 86 [hep-ph/0412058].

[47] S. Profumo, in preparation.

[48] P. Ullio, *Dark matter halos*, in proceedings of *The third international conference on frontier science, Monteporzio Catone (RM)*, Frascati Physics Series, P. Ullio ed., in preparation.

[49] J. Edsjo, M. Schelke and P. Ullio, *Direct versus indirect detection in mSUGRA with self-consistent halo models*, *JCAP* **09** (2004) 004 [astro-ph/0405414].

[50] J.F. Navarro, C.S. Frenk and S.D.M. White, *The structure of cold dark matter halos*, *Astrophys. J.* **462** (1996) 563 [astro-ph/9508025]; *A universal density profile from hierarchical clustering*, *Astrophys. J.* **490** (1997) 493;
J.S. Bullock et al., *Mon. Not. Roy. Astron. Soc* **321** (2001) 559 [astro-ph/astro-ph/9908159];
V.R. Eke, J.F. Navarro and M. Steinmetz, *The power spectrum dependence of dark matter halo concentrations*, *Astrophys. J.* **554** (2001) 114 [astro-ph/0012337].

[51] A. El-Zant, I. Shlosman and Y. Hoffman, *Dark halos: the flattening of the density cusp by dynamical friction*, *Astrophys. J.* **560** (2001) 336 [astro-ph/0103386].

[52] A. Burkert, *Type Ia supernova scenarios and the Hubble sequence*, Astrophys. J. 447199525 [astro-ph/9505090].

[53] P. Salucci and A. Burkert, *Dark matter scaling relations*, *Astrophys. J.* **537** (2000) L9 [astro-ph/0004397].

[54] G.R. Blumenthal, S.M. Faber, R. Flores and J.R. Primack, *Contraction of dark matter galactic halos due to baryonic infall*, *Astrophys. J.* **301** (1986) 27.

[55] P. Ullio, H.S. Zhao and M. Kamionkowski, *A dark-matter spike at the galactic center?*, *Phys. Rev.* **D 64** (2001) 043504 [astro-ph/0101481].

[56] J.F. Navarro et al., *The inner structure of lambdacdm halos III: universality and asymptotic slopes*, *Mon. Not. Roy. Astron. Soc.* **349** (2004) 1039 [astro-ph/0311231].

[57] B. Moore, et al., *Dark matter substructure within galactic halos*, *Astrophys. J.* **524** (1999) 19.

[58] A.S. Eddington, *The distribution of stars in globular clusters*, *MNRAS* **76** (1916) 572.

[59] CDMS collaboration, D.S. Akerib et al., *First results from the cryogenic dark matter search in the soudan underground lab*, *Phys. Rev. Lett.* **93** (2004) 211301 [astro-ph/0405033].

[60] E. Aprile et al., *The xenon dark matter search experiment*, Nucl. Phys. **138** *(Proc. Suppl.)* (2005) 156 [astro-ph/0407575].

[61] H. Baer, C. Balazs, A. Belyaev and J. O'Farrill, *Direct detection of dark matter in supersymmetric models*, *JCAP* **09** (2003) 007 [hep-ph/0305191].

[62] Super-Kamiokande collaboration, A. Habig, *An indirect search for wimps with super-kamiokande*, hep-ex/0106024.

[63] J. Edsjö, *Internal Amanda/IceCube report*, 2000.

[64] T. Sjostrand, *Pythia 5.7 and jetset 7.4: physics and manual*, hep-ph/9508391.

[65] F. Donato, N. Fornengo and P. Salati, *Antideuterons as a signature of supersymmetric dark matter*, *Phys. Rev.* **D 62** (2000) 043003 [hep-ph/9904481].

[66] L.J. Gleeson and W.I. Axford, *Cosmic rays in the interplanetary medium*, *Astrophys. J.* **149** (1967) L115

[67] A. Morselli, *Search for supersymmetric dark matter with GLAST*, Prepared for *8th International Conference on Advanced Technology and Particle Physics (ICATPP 2003): Astroparticle, Particle, Space Physics, Detectors and Medical Physics Applications*, Como, Italy, 6-10 Oct 2003.

[68] K. Mori et al., *A novel antimatter detector based on x-ray deexcitation of exotic atoms*, *Astrophys. J.* **566** (2002) 604 [astro-ph/0109463].

[69] C.J. Hailey et al., *Development of the gaseous antiparticle spectrometer for space-based antimatter detection*, *Nucl. Instrum. Meth.* **B214** (2004) 122–125 [astro-ph/0306589].

[70] F. Donato, N. Fornengo, D. Maurin and P. Salati, *Antiprotons in cosmic rays from neutralino annihilation*, *Phys. Rev.* **D 69** (2004) 063501 [astro-ph/0306207].

[71] L. Bergstrom, J. Edsjo and P. Ullio, *Cosmic antiprotons as a probe for supersymmetric dark matter?*, astro-ph/9902012.

[72] E.A. Baltz and J. Edsjo, *Positron propagation and fluxes from neutralino annihilation in the halo*, *Phys. Rev.* **D 59** (1999) 023511 [astro-ph/9808243].

[73] J.L. Feng, K.T. Matchev and F. Wilczek, *Prospects for indirect detection of neutralino dark matter*, *Phys. Rev.* **D 63** (2001) 045024 [astro-ph/0008115].

[74] D. Hooper and J. Silk, *Searching for dark matter with future cosmic positron experiments*, *Phys. Rev.* **D 71** (2005) 083503 [hep-ph/0409104].

[75] Galprop numerical package, http://www.mpe.mpg.de/~aws/propagate.html.

[76] N. Fornengo, L. Pieri and S. Scopel, *Neutralino annihilation into gamma-rays in the milky way and in external galaxies*, *Phys. Rev.* **D 70** (2004) 103529 [hep-ph/0407342].

[77] L. Bergstrom, P. Ullio and J.H. Buckley, *Observability of gamma rays from dark matter neutralino annihilations in the milky way halo*, *Astropart. Phys.* **9** (1998) 137 [astro-ph/9712318].

[78] P. Gondolo and J. Silk, *Dark matter annihilation at the galactic center*, *Phys. Rev. Lett.* **83** (1999) 1719 [astro-ph/9906391].

[79] A. Cesarini, F. Fucito, A. Lionetto, A. Morselli and P. Ullio, *The galactic center as a dark matter gamma-ray source*, *Astropart. Phys.* **21** (2004) 267 [astro-ph/0305075].

[80] WMAP collaboration, D.N. Spergel et al., *First year Wilkinson microwave anisotropy probe (wmap) observations: determination of cosmological parameters*, *Astrophys. J. Suppl.* **148** (2003) 175 [astro-ph/0302209].

[81] A. Bottino, F. Donato, N. Fornengo and S. Scopel, *Particle candidates for dark matter: a case for (dominant or subdominant) relic neutralinos*, hep-ph/0105233.

[82] B. Murakami and J.D. Wells, *Nucleon scattering with Higgsino and Wino cold dark matter*, *Phys. Rev.* **D 64** (2001) 015001 hep-ph/0011082;
T. Moroi and L. Randall, *Wino cold dark matter from anomaly-mediated SUSY breaking*, *Nucl. Phys.* **B 570** (2000) 455 hep-ph/9906527;
M. Fujii and K. Hamaguchi, *Higgsino and Wino dark matter from Q-ball decay in affleck-dine baryogenesis*, *Phys. Lett.* **B 525** (2002) 143 hep-ph/0110072; *Non-thermal dark matter via Affleck-Dine baryogenesis and its detection possibility*, *Phys. Rev.* **D 66** (2002) 083501 hep-ph/0205044;
R. Jeannerot, X. Zhang and R.H. Brandenberger, *Non-thermal production of neutralino cold dark matter from cosmic string decays*, *JHEP* **9912** (1999) 003 hep-ph/9901357;
W.B. Lin, D.H. Huang, X. Zhang and R.H. Brandenberger, *Non-thermal production of WIMPs and the sub-galactic structure of the Universe*, *Phys. Rev. Lett.* **86** (2001) 954 [astro-ph/0009003].

[83] P. Salati, *Quintessence and the relic density of neutralinos*, *Phys. Lett.* **B 571** (2003) 121 [astro-ph/0207396];
F. Rosati, *Quintessential enhancement of dark matter abundance*, *Phys. Lett.* **B 570** (2003) 5 [hep-ph/0302159].

[84] S. Profumo and P. Ullio, *SUSY dark matter and quintessence*, *JCAP* **11** (2003) 006 [hep-ph/0309220].

[85] R. Catena, N. Fornengo, A. Masiero, M. Pietroni and F. Rosati, *Dark matter relic abundance and scalar-tensor dark energy*, *Phys. Rev.* **D 70** (2004) 063519 [astro-ph/0403614].

[86] M. Kamionkowski and M.S. Turner, *Thermal relics: do we know their abundances?*, *Phys. Rev.* **D 42** (1990) 3310.

[87] S. Profumo, *Extended coannihilations from non universal sfermion masses*, hep-ph/0305040.

[88] See e.g.,M. Drees et al., *Scrutinizing lsp dark matter at the LHC*, *Phys. Rev.* **D 63** (2001) 035008 [hep-ph/0007202];
M. Battaglia, I. Hinchliffe and D. Tovey, *Cold dark matter and the LHC*, *J. Phys.* **G 30** (2004) R217 [hep-ph/0406147];
see also, http://physics.syr.edu/~trodden/lc-cosmology/.

[89] D.A. Dicus, S. Nandi and X. Tata, *W decay in supergravity guts*, *Phys. Lett.* **B 129** (1983) 451;
A.H. Chamseddine, P. Nath and R. Arnowitt, *Experimental signals for supersymmetric decays of the w and z bosons*, *Phys. Lett.* **B 129** (1983) 445;
H. Baer and X. Tata, *Multi - lepton signals from w+- and z0 decays to gauginos at $\bar{p}p$ colliders*, *Phys. Lett.* **B 155** (1985) 278;
H. Baer, K. Hagiwara and X. Tata, *Can the CERN $p\bar{p}$ collider limit gaugino masses?*, *Phys. Rev. Lett.* **57** (1986) 294;
R. Arnowitt and P. Nath, *Supersymmetric signals at the Tevatron*, *Mod. Phys. Lett.* **A 2** (1987) 331;
R. Barbieri, F. Caravaglios, M. Frigeni and M.L. Mangano, *Production and leptonic decays of charginos and neutralinos in hadronic collisions*, *Nucl. Phys.* **B 367** (1991) 28;
H. Baer and X. Tata, *Probing charginos and neutralinos beyond the reach of lep at the Tevatron collider*, *Phys. Rev.* **D 47** (1993) 2739;
J.L. Lopez, D.V. Nanopoulos, X. Wang and A. Zichichi, *Supersymmetry tests at fermilab: a proposal*, *Phys. Rev.* **D 48** (1993) 2062 [hep-ph/9211286];
H. Baer, C. Kao and X. Tata, *Aspects of chargino - neutralino production at the Tevatron collider*, *Phys. Rev.* **D 48** (1993) 5175 [hep-ph/9307347];
S. Mrenna, G.L. Kane, G.D. Kribs and J.D. Wells, *Possible signals of constrained minimal supersymmetry at a high luminosity fermilab Tevatron collider*, *Phys. Rev.* **D 53** (1996) 1168 [hep-ph/9505245];
H. Baer, C.-h. Chen, F. Paige and X. Tata, *Supersymmetry reach of Tevatron upgrades: a comparative study*, *Phys. Rev.* **D 54** (1996) 5866 [hep-ph/9604406];
K.T. Matchev and D.M. Pierce, *New backgrounds in trilepton, dilepton and dilepton plus tau jet SUSY signals at the Tevatron*, *Phys. Lett.* **B 467** (1999) 225 [hep-ph/9907505];
H. Baer, M. Drees, F. Paige, P. Quintana and X. Tata, *Trilepton signal for supersymmetry at the fermilab Tevatron revisited*, *Phys. Rev.* **D 61** (2000) 095007 [hep-ph/9906233];
V.D. Barger, C. Kao and T.-j. Li, *Trilepton signal of minimal supergravity at the Tevatron including tau-lepton contributions*, *Phys. Lett.* **B 433** (1998) 328 [hep-ph/9804451];
V.D. Barger and C. Kao, *Trilepton signature of minimal supergravity at the upgraded Tevatron*, *Phys. Rev.* **D 60** (1999) 115015 [hep-ph/9811489].

[90] H. Baer, T. Krupovnickas and X. Tata, *Reach of the Fermilab Tevatron for minimal supergravity in the region of large scalar masses*, *JHEP* **07** (2003) 020 [hep-ph/0305325].

[91] H. Baer, C. Balazs, A. Belyaev, T. Krupovnickas and X. Tata, *Updated reach of the CERN LHC and constraints from relic density, $b \to s\gamma$ and A_μ in the mSUGRA model*, *JHEP* **0306** (2003) 054 [hep-ph/0304303];
for earlier work, see H. Baer, C.H. Chen, F. Paige and X. Tata, *Signals for minimal supergravity at the CERN large hadron collider: multi-jet plus missing energy channel*, *Phys. Rev.* **D 52** (1995) 2746 [hep-ph/9503271]; *Signals for minimal supergravity at the CERN large hadron collider II: multilepton channels*, *Phys. Rev.* **D 53** (1996) 6241 [hep-ph/9512383] H. Baer, C. Balazs, A. Belyaev, T. Krupovnickas and X. Tata, *Updated reach of the cern LHC and constraints from relic density, $b \to s\gamma$ and A_μ in the mSUGRA model*, *JHEP* **06** (2003) 054 [hep-ph/0304303];
H. Baer, C.-h. Chen, M. Drees, F. Paige and X. Tata, *Probing minimal supergravity at the cern LHC for large* $\tan\beta$, *Phys. Rev.* **D 59** (1999) 055014 [hep-ph/9809223];
S. Abdullin and F. Charles, *Search for SUSY in (leptons +) Jets + $E_T^{\rm mis}$s final states*, *Nucl. Phys.* **B 547** (1999) 60 [hep-ph/9811402];
CMS collaboration, S. Abdullin et al., *Discovery potential for supersymmetry in CMS*, *J. Phys.* **G 28** (2002) 469 [hep-ph/9806366];
B. Allanach, J. Hetherington, A. Parker and B. Webber, *Naturalness reach of the large hadron collider in minimal supergravity*, *JHEP* **08** (2000) 017 [hep-ph/0005186].

[92] D. Denegri et al., *Summary of the CMS discovery potential for the MSSM SUSY higgses*, [hep-ph/0112045];
F. Moortgat, S. Abdullin and D. Denegri, *Observability of MSSM Higgs bosons via sparticle decay modes in CMS*, [hep-ph/0112046].

[93] H. Baer, M. Bisset, X. Tata and J. Woodside, *Supercollider signals from gluino and squark decays to Higgs bosons*, *Phys. Rev.* **D 46** (1992) 303;
F. Moortgat, S. Abdullin and D. Denegri, *Observability of MSSM Higgs bosons via sparticle decay modes in CMS*, [hep-ph/0112046];
A. Datta, A. Djouadi, M. Guchait and Y. Mambrini, *Charged Higgs production from SUSY particle cascade decays at the LHC*, *Phys. Rev.* **D 65** (2002) 015007 [hep-ph/0107271];
A. Datta, A. Djouadi, M. Guchait and F. Moortgat, *Detection of MSSM Higgs bosons from supersymmetric particle cascade decays at the LHC*, *Nucl. Phys.* **B 681** (2004) 31 [hep-ph/0303095].

[94] C. Kao and N. Stepanov, *Discovering the Higgs bosons of minimal supersymmetry with muons*, *Phys. Rev.* **D 52** (1995) 5025 [hep-ph/9503415];
S. Dawson, D. Dicus, C. Kao and R. Malhotra, *Discovering the Higgs bosons of minimal supersymmetry with muons and a bottom quark*, *Phys. Rev. Lett.* **92** (2004) 241801 [hep-ph/0402172].

[95] H. Baer, V.D. Barger, D. Karatas and X. Tata, *Detecting gluinos at hadron supercolliders*, *Phys. Rev.* **D 36** (1987) 96.

[96] Atlas collaboration, *Atlas detector and physics performance: technical design report*, LHCC 99-14/15.

[97] H. Baer, T. Krupovnickas and X. Tata, *Two photon background and the reach of a linear collider for supersymmetry in wmap favored coannihilation regions*, *JHEP* **06** (2004) 061 [hep-ph/0405058].

[98] V.D. Barger, T. Han and J. Jiang, $\tan\beta$ *determination from heavy Higgs boson production at linear colliders*, *Phys. Rev.* **D 63** (2001) 075002 [hep-ph/0006223].

JHEP07(2005)065

[99] H. Baer, B.W. Harris and X. Tata, *The reach of cern lep2 and fermilab Tevatron upgrades for Higgs bosons in supersymmetric models*, *Phys. Rev.* **D 59** (1999) 015003 [hep-ph/9807262].

[100] M. Carena, S. Mrenna and C.E.M. Wagner, *MSSM Higgs boson phenomenology at the Tevatron collider*, *Phys. Rev.* **D 60** (1999) 075010 [hep-ph/9808312];
Higgs Working Group collaboration, M. Carena et al., *Report of the Tevatron Higgs working group*, hep-ph/0010338.

[101] H. Baer, C.-h. Chen, F. Paige and X. Tata, *Detecting sleptons at hadron colliders and supercolliders*, *Phys. Rev.* **D 49** (1994) 3283 [hep-ph/9311248].

[102] CDF collaboration, T. Affolder et al., *Search for scalar top and scalar bottom quarks in $p\bar{p}$ collisions at $\sqrt{s} = 1.8$ tev*, *Phys. Rev. Lett.* **84** (2000) 5704 [hep-ex/9910049].

[103] H. Baer, M. Bisset, D. Dicus, C. Kao and X. Tata, *The search for Higgs bosons of minimal supersymmetry: impact of supersymmetric decay modes*, *Phys. Rev.* **D 47** (1993) 1062;
H. Baer, M. Bisset, C. Kao and X. Tata, *Detecting Higgs boson decays to neutralinos at hadron supercolliders*, *Phys. Rev.* **D 50** (1994) 316 [hep-ph/9402265];
G. Belanger, F. Boudjema, F. Donato, R. Godbole and S. Rosier-Lees, *SUSY Higgs at the LHC: effects of light charginos and neutralinos*, *Nucl. Phys.* **B 581** (2000) 3 [hep-ph/0002039];
M. Bisset, M. Guchait and S. Moretti, *Signatures of MSSM charged Higgs bosons via chargino neutralino decay channels at the LHC*, *Eur. Phys. J.* **C 19** (2001) 143 [hep-ph/0010253];
M. Bisset et al., *Pair-produced heavy particle topologies: mSSM neutralino properties at the LHC from gluino/squark cascade decays*, hep-ph/0501157.

[104] S.Y. Choi et al., *Reconstructing the chargino system at e^+e^- linear colliders*, *Eur. Phys. J.* **C 14** (2000) 535 [hep-ph/0002033].

[105] J.L. Feng and D.E. Finnell, *Squark mass determination at the next generation of linear e^+e^- colliders*, *Phys. Rev.* **D 49** (1994) 2369 [hep-ph/9310211].

[106] G. Anderson, H. Baer, C.-h. Chen and X. Tata, *The reach of fermilab Tevatron upgrades for* SU(5) *supergravity models with non-universal gaugino masses*, *Phys. Rev.* **D 61** (2000) 095005 [hep-ph/9903370].

[107] H. Baer, C.-h. Chen, M. Drees, F. Paige and X. Tata, *Collider phenomenology for supersymmetry with large* $\tan\beta$, *Phys. Rev. Lett.* **79** (1997) 986 [hep-ph/9704457].

JHEP07(2005)065